A syngeneic spontaneous zebrafish model of *tp53*-deficient, EGFR^{viii}, and PI3KCA^{H1047R}-driven glioblastoma reveals inhibitory roles for inflammation during tumor initiation and relapse *in vivo*

Alex Weiss[1], Cassandra D'Amata[1], Bret J. Pearson[3,4*], Madeline N. Hayes[1,2*]

[1]Developmental and Stem Cell Biology Program, The Hospital for Sick Children, Toronto, Canada
[2]Department of Molecular Genetics, University of Toronto, Toronto, Canada
[3] Knight Cancer Institute, Oregon Health & Science University, Portland, Oregon, 97239, USA
[4] Department of Pediatrics, Papé Research Institute, Oregon Health & Science University, Portland, Oregon, 97239, USA

*Correspondence:

Madeline N. Hayes
The Hospital for Sick Children PGCRL Building
686 Bay Street, Toronto, Ontario
M5G 0A4, Canada
Phone: 416-813-7654, ext. 328370
E-mail: madeline.hayes@sickkids.ca

Bret J. Pearson
3181 SW Sam Jackson Park Rd.
LBRB Room 305, L481
Portland, OR, 97239, USA
503-494-7979
E-mail: pearsobr@ohsu.edu

Keywords: Glioblastoma, Zebrafish, Oncogenesis, Tumor microenvironment

Disclosure of Potential Conflicts of Interest:
The authors declare no potential conflicts of interest.

Abstract

To build a patient-relevant *in vivo* model of human glioblastoma, we expressed common oncogenic variants including activated human EGFR[viii] and PI3KCA^{H1047R} under the control of the radial glial-specific promoter *her4.1* in syngeneic *tp53* loss-of-function mutant zebrafish. Robust tumor formation was observed prior to 45 days of life, with a gene expression signature similar to human glioblastoma of the mesenchymal subtype, along with a strong inflammatory component. Within early stage tumor lesions, and in an intact and endogenous tumor microenvironment, we visualized infiltration of phagocytic cells, as well as internalization of tumor cells by *mpeg1.1*:GFP+ microglia/macrophages, suggesting negative regulatory pressure by pro-inflammatory cell types on tumor growth at early stages of glioblastoma initiation *in vivo*. Furthermore, CRISPR/Cas9-mediated gene targeting of master inflammatory transcription factors *irf7* and *irf8* led to increased tumor formation in the primary context, while suppression of microglial/macrophage activity led to enhanced tumor cell engraftment following transplantation into otherwise immune competent zebrafish hosts. Altogether, we developed a genetically-relevant model of aggressive human glioblastoma and harnessed the unique advantages of zebrafish including live imaging, high-throughput genetic and chemical manipulations to highlight important tumor suppressive roles for the innate immune system on glioblastoma initiation, with important future significance for therapeutic discovery and optimizations.

Introduction

Brain tumors comprise a diverse set of malignancies that develop from brain tissue or from metastatic cancer cells that have spread from other primary sites throughout the body. Glioblastoma represents a common type of primary brain cancer and represents about 50% of all primary brain malignancies in adults[1,2]. Despite intensive treatments including surgery, radiation, and chemotherapy (temozolomide, TMZ), the vast majority of patients eventually relapse, with a median survival rate of less than 15 months[3]. Therapeutic resistance can partly be attributed to a poor understanding of underlying molecular mechanisms, as well as a significant level of genetic heterogeneity between patients. Plasticity among tumor and non-tumor cells within individual patient tumors also contributes to complex tumor cell evolution over time. Heterogeneity within glioblastoma is observed at several levels, including genetic, transcriptional, and DNA methylation, which is increasingly important for classification and characterization of major molecular subtypes including proneural, classical, and mesenchymal[2,4–6]. These categories reflect dominant oncogenic drivers, gene expression profiles, and prognoses, with mesenchymal-type glioblastomas having the poorest outcome, characterized by upregulation of angiogenesis genes and pathways involved in cell invasion[7]. Interestingly, single cell sequencing has identified the co-existence of different glioblastoma subtypes within individual tumors[8–10], revealing less distinct separations between molecular subtypes and an underlying cellular flexibility contributing to tumor aggressiveness and drug resistance.

Much of the cellular flexibility in glioblastoma is influenced by the tumor microenvironment (TME), which is highly complex consisting of various resident brain, stroma, and immune cells,

as well as cells recruited from the general circulation such as bone marrow-derived immune cells with known tumor suppressive and tumor promoting functions[11,12]. Given emerging opportunities for harnessing the immune system for the treatment of human cancer, there is a growing focus on understanding innate and adaptive immune responses across different subtypes of human malignancies. However, like many other tumors, glioblastoma combines a lack of immunogenicity due to few mutations with a highly immunosuppressive tumor microenvironment. In addition to off-target effects of current frontline therapeutic strategies, both tumor and immune cells contribute to immune suppression in and surrounding the TME[13,14], which could explain the failure of immunotherapy-based clinical trials in glioblastoma. Additionally, lymphocytes are frequently exhausted and dysfunctional and therefore inadequate at exerting an anti-tumor immune response, while tumor-associated myeloid cells are frequently reprogrammed by signaling from tumor cells and the TME to cell states that promote glioblastoma survival, growth and invasion[13,15,16]. Evidence also supports tumor-cell intrinsic mechanisms in response to immune cell attack leading to various evasion mechanisms, including upregulation of myeloid-associated gene expression programs and resistance to interferon signaling[17,18]. Altogether, evidence suggests a complexity of inter-cellular signaling pathways that modify the behavior of both tumor and non-tumor cells within the TME, contributing to glioblastoma progression in patients.

Intercellular communication in glioblastoma highlights the importance of faithful *in vivo* models. However, given a historical lack of tractable and immunocompetent vertebrate animal model systems for glioblastoma gene discovery and drug screening, roles for the endogenous TME especially at early stages of tumor initiation, remain poorly understood. Furthermore, live visualization of heterogeneity and tumor cells within the TME is limited in non-transparent rodent

genetic models and/or patient-derived tumor xenografted hosts. Therefore, our goal was to develop a patient-relevant model of aggressive human glioma in an intact and immune competent vertebrate animal model system. We developed a novel spontaneous, syngeneic zebrafish model of mesenchymal-like glioblastoma, with high levels of inflammatory immune cell infiltration and anti-tumor associations between microglia/macrophages and tumor cells, suggesting inhibitory roles for inter-cellular interactions during glioblastoma initiation and an effective *in vivo* platform for future biological discovery and drug testing for patients.

Results

Oncogenic MAPK/AKT pathway activation drives glial-derived tumor formation in syngeneic *tp53* mutant zebrafish

The RTK/RAS/PI3K pathway is a key driver of tumorigenesis across human cancers, and 90% of glioblastoma tumors exhibit alterations in core signaling pathway genes[4,19]. Some of the most frequent genetic alterations in glioblastoma include activating mutations and/or amplifications of the Epidermal Growth Factors Receptor (EGFR) tyrosine kinase; loss of the lipid phosphatase PTEN, which antagonizes the phosphatidylinositol-3 kinase (PI3K) pathway; and/or activating mutations in the PI3K catalytic subunit PIK3CA, which altogether drive downstream activation of oncogenic RAS/MAPK and AKT/mTOR signaling pathway activity[4,19]. Furthermore, the TP53 tumor suppressor pathway is altered in 84% of globlastoma patients and 94% of cell lines, with TP53 loss implicated in proliferation, invasion, migration, and stemness[4,19,20]. Importantly, single pathway mutations are generally insufficient to transform normal brain tissues, and multiple mutations are required for glioma formation[21–24]. Therefore, to recapitulate human glioblastoma

in vivo, multiple genetic events should be considered for translational modeling to activate oncogenic signaling pathways involved in the aggressive tumor cell behaviors seen in patients.

To generate a patient-relevant brain tumor model in zebrafish we used the zebrafish *her4.1* promoter to simultaneously over-express constitutively-active human EGFR ($EGFR^{vIII}$) and PI3KCA ($PI3KCA^{H1047R}$) variants in neural progenitors and radial glia of syngeneic *tp53* loss-of-function mutant larvae[21,25,26]. Co-injection of linearized *her4.1*:**E**GFR^{viii} + *her4.1*:**P**$I3KCA^{H1047R}$ + *her4.1*:m**S**carlet transgenes into syngeneic (CG1) *tp53*$^{-/-}$ mutant embryos at the one-cell stage led to broad transient mScarlet expression for 2-3 days followed by rare mosaic expression in the anterior CNS (henceforth referred to as p53EPS, Fig 1A), as expected from this transient mosaic injection strategy used to express stable concatemers of DNA vectors[27]. Starting at 15 days post fertilization (dpf), this transgene combination led to visible mScarlet-positive brain lesions in the anterior CNS of live zebrafish (Fig 1B-D). Injections of single linearized vector and vector combinations resulted in a maximum incidence of approximately 15-20% affected zebrafish induced by the p53EPS combination by 45 dpf (Fig 1D). Inter-tumoral variability was observed among p53EPS mosaic-injected zebrafish, with tumors of variable size arising in different brain regions including telecephalon and diencephalon regions (~28%), and the optic tectum/mesencephalon region (~72%) (Supplementary Fig 1). To further define the tissue of origin of zebrafish p53EPS CNS lesions, we co-injected linearized *gfap*:EGFP[28] and visualized EGFP expression in 100% of brain masses at 30-40 dpf (Fig 1A,B), supporting glial identity and novel *in vivo* model of malignant glioma.

To test for transformation of p53EPS cells from primary mosaic-injected animals, we harvested bulk tissue from dissected zebrafish brains and transplanted dissociated cells into the hindbrain

ventricles of 2 dpf syngeneic *tp53* wild-type (CG1) zebrafish[29]. At approximately 18 days post-transplant (18 dpt, or 20 dpf), we screened for mScarlet+ fluorescence and visualized her4.1+/gfap+ tumor cell outgrowth in transplanted host (Fig 1E,F), supporting oncogenic transformation and malignant growth *in vivo* of p53EPS cells. Fluorescence activated cell sorting (FACS) revealed fluorescently labeled tumor cells in un-labeled sygeneic host brains and co-expression of *her4.1*:mScarlet/*gfap*:EGFP (Fig 1G), further supporting tumor growth from a glial-derived progenitor cell, which was expected from *her4.1*-specific oncogene activation during early stages of zebrafish development[25].

We performed sectioning of primary p53EPS zebrafish and visualized highly proliferative forebrain and optic tectum/mesencephalon lesions that stained positive for phosphorylated-ERK and phosphorylated-AKT (Fig 1H-K), confirming activation of downstream MAPK and AKT signaling pathways, respectively. To validate effects of relevant downstream signaling pathway activation, we co-injected linearized *her4.1*:**K**RAS^{G12D} + *her4.1*:**P**I3KCA^{H1047R} + *her4.1*:m**S**carlet into CG1*tp53*$^{-/-}$ embryos (p53KPS). Starting at 15-20 dpf, we visualized tumor onset and penetrance comparable to p53EPS (Supplementary Figure 2), suggesting a dominant role for MAPK/AKT pathway activation downstream of RTK signaling in driving tumor formation, and a flexible oncogenic strategy for driving robust brain tumor formation in zebrafish.

RNA expression analysis establishes enrichment of human mesenchymal glioblastoma signatures and gene expression patterns associated with inflammation.

To further characterize our novel zebrafish brain tumor models, we performed bulk RNA sequencing (RNAseq) of three independent p53EPS tumor-burdened brains, three independent

p53KPS tumor-burdened brains, and three age-matched control-injected zebrafish brains that remained tumor-free at the time of harvesting tissue. Using hierarchical clustering on normalized gene expression, our tumor-free control samples clustered together and apart from p53EPS and p53KPS tumor brains, which displayed a recognizable level of transcriptional variability across principal components (Fig 2A). Interestingly, p53EPS and p53KPS samples failed to cluster according to oncogenic drivers (Fig 2A), suggesting molecular similarities as well as inter-tumor heterogeneity reflecting differences in tumor location, size, and contribution of tumor cells to total sample inputs.

Given the increased oncogenic relevance of our p53EPS driver combination to human glioblastoma, we chose to focus the remainder of our molecular analyses on p53EPS samples. Using differential gene expression analysis, we identified a conserved set of differentially expressed (DE) genes in p53EPS tumor brains, with 236 upregulated and 28 downregulated genes, compared to control injected brains at 20-30 dpf ($2 > \log2foldChange > -2$, adjusted *p*-value < 0.05, Supplementary Table 1, Fig 2B). Using DE genes, we identified human orthologs (Supplementary Table 2) and performed Gene Set Enrichment Analysis (GSEA)[30,31] comparing our p53EPS zebrafish model to published expression patterns for human glioblastoma subtypes, as well as embryonal brain tumors including designated subtypes of medulloblastoma[6,19,32]. Among these gene sets, we found a significant enrichment for the mesenchymal subtype of human glioblastoma in p53EPS differentially expressed genes (Fig 2C)[6,19]. In contrast, no significant enrichment was found for signatures associated with classical glioblastoma, proneural glioblastoma, Shh, Wnt, Group 3 or Group 4 medulloblastoma (Supplementary Fig 3)[6,19,32]. Together with the selected oncogenic drivers used to induce tumor formation *in vivo*, expression data supports significant molecular similarity between our

zebrafish p53EPS brain tumor model and human glioblastoma, specifically of the mesenchymal subtype. To further assess potential underlying molecular mechanisms, we also used our p53EPS DE signature to unbiasedly assess Hallmark gene sets available through the Molecular Signature Database (MSigDB, Supplementary Table 3)[33]. Interestingly, 7 of the top 13 enriched gene sets (NOM p-value <0.05) related to inflammation or inflammatory signaling pathways, including the Interferon gamma response, TNFA signaling, the Interferon alpha response, and Jak/STAT3 signaling (Fig 2D, Supplementary Table 3), suggesting a strong inflammatory component in our model. Additional pathway signatures included those related to RAS signaling, Hypoxia, and Epithelial-to-Mesenchymal Transitions (EMT) (Supplementary Table 3), suggesting on target oncogenic pathway activation, hypoxia, and invasive properties, consistent with aggressive glioblastoma[34,35].

Given the *in vivo* context and contribution of tumor and non-tumor cell types to our bulk RNAseq analysis, we decided to assess RNA expression in FACS sorted *her4.1:*mScarlet+ tumor cells, as well as *her4.1*:mScarlet-negative bulk stromal cells, compared to non-tumor whole brain tissue (Fig 2E, Supplementary Table 4). Interestingly, we observed increased immune cell and inflammatory gene expression in both p53EPS tumor and stromal cell fractions compared to control unaffected whole brain tissue, including transcripts associated with myeloid cell types (*mpeg1, irf7, irf8*), lymphoid genes (*rag1, rag2, lck*), *stat1a/b*, *fas* cell surface death receptor, and toll-like receptor 4b (*tlr4bb*), among others genes involved in immune responses (adjusted p-value < 0.0001, Fig 2E, Supplementary Table 4). We validated a selection of genes from RNAseq using RT-PCR (Supplementary Fig 4), as well as transient co-injection of linearized transgene with our EPS mix to assess tumor cell-specific expression of lymphoid *rag2*:EGFP and myeloid *mpeg1.1:*EGFP at 30 dpf (Fig 2F-I). Interestingly, we observed co-expression of

her4.1:mScarlet/*rag2*:EGFP and *her4.1*:mScarlet/*mpeg1.1*:EGFP in p53EPS tumor-burdened brains (Fig 2F-I), suggesting promoter activity at certain immune-associated genes within established p53EPS tumor cells *in vivo.* These data suggest inflammation-associated gene expression in both zebrafish glioblastoma-like cells and the tumor microenvironment and is consistent with inflammatory gene expression in tumor cells associated with immune evasion and *in vivo* growth in other models[17,36]. Together, we conclude that the p53EPS zebrafish is a comparable and relevant model system to study glioblastoma tumor biology, as well as intercellular interactions within an endogenous TME.

Zebrafish mesenchymal glioblastoma-like tumors recruit activated mononuclear phagocytes at early stages of tumor formation

Given that p53EPS tumor-burdened brains had strong enrichment for transcriptional signatures associated with inflammation, we were interested in the role for innate immune cells in the earliest stages of p53EPS tumor formation. Myeloid cells including microglia and macrophages are recruited in many different subtypes of primary brain tumors and in brain metastases[37,38]. However, how mononuclear phagocyte populations affect glioblastoma initiation is less well understood given that most studies utilize established tumor cell models and/or patient derived tissue xenografts. To assess whether myeloid-derived phagocytic cell lineages are enriched in p53EPS lesions at early stages of tumor initiation, we first used histological neutral red staining that labels lysosomal-rich phagocytes[39,40]. We observed enrichment of neutral red-positive foci in regions of *her4.1*:mScarlet+ fluorescent intensity as early as 10 dpf (Fig 3A), suggesting phagocyte infiltration during p53EPS initiation, prior to observation of macroscopic tumor masses (Fig 1D). We also co-injected our oncogene combination into *tp53*$^{-/-}$

embryos carrying a Tg(*tnfa*:EGFP) transgenic marker of activated phagocytes[41], and observed enrichment of *tnfa*:EGFP single-positive cells in *her4.1*:mScarlet+ lesions at 10-15 dpf (Fig 3B), suggesting the presence of activated and what normally would be considered tumor suppressive phagocytic cells at the site of p53EPS initiations[41,42].

Given that *tnfa* is a consensus marker of M1-polarized/activated macrophages, and that Tg(*tnfa*:EGFP) was previously found to label majority *mpeg1*+ macrophages *in vivo* following injury and infection[41,42], we decided to look more closely at microglia/macrophages cell dynamics *in vivo* using live confocal imaging following co-injection of our *her4.1*:EPS linearized transgene combination into *tp53*$^{-/-}$; Tg(*mpeg1.1*:EGFP) zebrafish[43]. At 10-15 dpf in p53EPS zebrafish, we observed fluorescent *mpeg1.1:*EGFP+ cells surrounding and within regions of concentrated *her4.1*:mScarlet+ fluorescence (Fig 3C, Movie 1). Microglia/macrophages outside of early-stage *her4.1:*mScarlet+ lesions displayed highly ramified morphologies, with several processes that were extended and retracted, indicative of environmental surveillance (Fig 3C, Movie 1)[44]. *mpeg1.1:*EGFP+ microglia/macrophages infiltrated into dense *her4.1:*mScarlet+ regions displayed more rounded and amoeboid-like morphology, supporting their activation in association with p53EPS oncogenic cells[45]. Interestingly, *mpeg1.1:*EGFP+ microglia/macrophages dynamically interacted with *her4.1*:mScarlet+ cells (Movies 1-2), and in early stage p53EPS oncogenic masses, *mpeg1.1:*EGFP+ microglia/macrophages associated closely with and often displayed internalized *her4.1:*mScarlet+ punctate cells (Fig 3C,D), suggesting engulfment and removal of p53EPS cells during tumor formation *in vivo*. Altogether, visualization of infiltrating myeloid-derived immune cells in p53EPS glioblastoma-like lesions, dynamic microglia/macrophages-p53EPS interactions, and tumor cell engulfment suggests anti-tumoral activity at early stages that could negatively affect tumor formation *in vivo*.

Inflammation-associated *irf7* and *irf8* are required to inhibit p53EPS tumor formation *in vivo*

Interferon regulatory factor (Irf) proteins regulate transcription of interferon genes, supporting immune reposes. Irf7 and Irf8 are critical for global activation of the type I IFN response following stimulation and for myeloid cell development, respectively[40,46,47]. Irf8 is a conserved determinant of macrophage cell fate during hematopoiesis and *irf8* mutant zebrafish lack microglia/macrophages in the brain up to 31 dpf[40]. Irf7 also drives differentiation of macrophages; however, in zebrafish and other systems, Irf7 is more broadly activated in immune cells in response to infection, with emerging evidence showing non-immune cell-related functions during development and cancer progression[17,36,46–49]. Interestingly, we observed upregulation of several interferon regulatory factor (Irf) family members including *irf7* and *irf8* in p53EPS tumor-burdened brains (Fig 2, Supplementary Tables 2 & 4), suggesting potential roles for these master regulators of inflammation on specific immune-related responses during p53EPS tumorigenesis *in vivo*. Therefore, to define functional roles for Irf7 and Irf8 in p53EPS formation, we used a transient CRISPR/Cas9 gene targeting approach to knock-down *irf7* and *irf8* genes prior to p53EPS tumor formation through co-injection of 2-3 gRNAs targeting *irf7* or *irf8* (Supplementary Table 5), together with Cas9 protein and linearized EPS into one-cell stage *tp53*$^{-/-}$ embryos. At 2-5 dpf, we extracted DNA from a subset of injected embryos and observed a gene targeting efficiency of >90% and >65% INDELS at the *irf7* and *irf8* loci, respectively (ICE analysis, Synthego, ice.synthego.com)[50]. Gene transcript knock-down was also verified using RT-PCR (Supplementary Fig 5). Consistent with previous reports, *irf8* knock-down resulted in significant reductions in neutral red-positive phagocytes at 8-10 dpf (Supplementary Fig 6)[40],

and while no significant differences in neutral red-positive phagocyte number were observed following *irf7* gene targeting, *irf7* CRISPR/Cas9-injected animals displayed early mortality un-related to brain tumor formation, with ~80% of our colony displaying illness prior to two months of age, consistent with a broad requirement for Irf7 in immune responses, among other functions.

Remarkably, following *irf7* and *irf8* gene knock-down with p53EPS, we observed robust tumor formation, with 65% of *irf7*-targeted and 42% of *irf8*-targeted p53EPS zebrafish developing tumors by 30 dpf, compared to 20% p53EPS incidence (Fig 4A-D, *irf7* $p<0.0001$, *irf8* $p=0.0155$, Fisher's exact test), suggesting an important inhibitory role for *irf7* and *irf8* in p53EPS tumor initiation. In p53EPS tumor brains with *irf7* and *irf8* knock-down, we observed reduced expression of genes associated with our inflammation signature in p53EPS tumor-burdened brains, including immune evasion-associated transcripts like *suppressor of cytokine signaling 1a* (socs1a) (Supplementary Fig 5), suggesting reduced tumor-associated inflammation and associated immune-evasion mechanisms, which were previously shown to be upregulated in response to anti-tumor cell infiltration[17].

Given reports of *IRF7* gene expression in human glioblastoma tumor cells, association with worsened patient outcome, and potential roles in tumor stem cell biology[51,52], we decided to investigate tumor cell-specific roles for *irf7* in p53EPS initiation. To specifically knock-down *irf7* in p53EPS tumor cells, we generated a transgenic Tg(*her4.1*:Cas9-2A-EGFP);*tp53*$^{-/-}$ zebrafish strain and co-injected embryos with linearized EPS + gRNAs targeting *irf7* (Fig 4E). Despite a gene targeting efficiency of ~28% in pooled tumor cells from 5 tumor-burdened animals, we did not observe any significant changes in p53EPS tumor formation in Cas9-2A-EGFP-positive

zebrafish compared to Cas9-2A-EGFP-negative control injected siblings (Fig 4E-G). We observed similar effects following co-injection of gRNAs targeting *irf8* (Fig 4G), suggesting that increased p53EPS tumor initiation following *Irf* gene knock-down is a consequence of *irf7* and *irf8* loss-of-function in the TME.

Macrophages are required to suppress p53EPS engraftment following transplant into syngeneic zebrafish hosts

Given a conserved role for *irf8* in resident microglia and macrophage development across species[40], our functional data suggests an anti-tumor role for *irf/*macrophage activity in the TME during p53EPS tumor initiation. To further assess the role for microglia/macrophages during re-initiation of p53EPS following transplantation, we injected p53EPS tumor cells into the hindbrain ventricle of syngeneic host embryos at 2 dpf along with Clodronate liposomes (Clodrosomes), a chemical commonly used to eliminate macrophages[53–55]. At 18 days post-transplant (20 dpf), we observed 50% p53EPS tumor cell engraftment in host animals co-injected with Clodronate liposomes, compared to 23% injected with vehicle control liposomes (p=0.0048, Fisher's exact test, Fig 5A-C). Interestingly, while p53EPS engrafted brains maintained inflammatory gene expression patterns, similar to primary p53EPS tumor-burdened brains (Supplementary Fig 7A), co-transplantation with Clodrosomes inhibited inflammatory gene expression in bulk tissue (Supplementary Fig 7B, normalized to mScarlet expression to control for differences in tumor size), suggesting that reduced microglia/macrophage-driven inflammation supports p53EPS tumor cell engraftment and growth following transplantation into syngeneic host zebrafish. We also performed p53EPS bulk tumor cell transplantations into the hindbrain ventricles of *irf8* CRISPR/Cas9-injected syngeneic host zebrafish embryos at 2 dpf, and observed 46% p53EPS

tumor cell engraftment at 20 dpf, compared to 19% engraftment in *irf8* wild-type host zebrafish (p=0.0002, Fisher's exact test, Fig 5D), supporting an inhibitory role for microglia/macrophages in the TME and p53EPS tumor cell engraftment. Altogether, our modeling data using patient-relevant oncogene combination in *tp53* loss-of-function background demonstrates an important role for inflammation in glioblastoma initiation and relapse including inhibitory roles for Irf-dependent signaling pathways, which in part may be attributed to anti-tumoral macrophage activity within the TME.

Discussion

Creating faithful models and discovering tailored treatments for glioblastoma patients has resulted in many different experimental platforms, each with their own unique advantages and experimental challenges[58,59]. Genetically engineered mouse models (GEMM) are widely used for the study of tumorigenesis in a physiological context; however, most cannot fully recapitulate genetic heterogeneity in a timely and cost-effective manner and are therefore limited in the context of preclinical drug testing. Patient-derived xenografts (PDX) resemble patient tumors more closely as they retain mutational heterogeneity; however, PDX models cannot be used to address mechanisms of tumor onset in an intact and endogenous tumor microenvironment given that they are derived from pre-evolved tumor tissue and are either studied *ex vivo* or engrafted into immune-deficient animal hosts. Human stem cell-derived organoids represent a great advance in the field for the study of tumor development and for screening new therapeutic strategies, but the lack of an intact TME excludes both known and unknown inter-cellular interactions, which are increasingly appreciated to influence tumor cell evolution and drug responses in patients.

Zebrafish are a well-established and robust model for studying human cancer pathobiology and are well suited for screening novel targeted therapies *in vivo*. Zebrafish models of human brain tumors have been generated previously using transgenic overexpression of human oncogenes or xenograft transplantation of patient-derived tumor cells into zebrafish larvae[60–63], and these models have proven useful for defining important molecular pathways in glioma transformation, tumor growth and migration. However, most of these available zebrafish models are induced using single oncogenic drivers driven by a variety of neuronal and/or glial-specific promoters at different time points throughout development, with the use of single oncogenes in a functional *tp53* signaling background likely contributing their inability to model highly aggressive and relapse-like phenotypes *in vivo*. Xenograft transplantations of human glioblastoma cells into zebrafish larvae omits a fully functional immune system, which our work suggests plays an important role on tumor initiation and growth both in the primary context and following p53EPS tumor cell transplantation. Therefore, our zebrafish model of aggressive and transplantable human glioblastoma represents an exciting opportunity to study important aspects related to tumor cell progression and relapse in an intact and endogenous TME. Using widely used markers of innate immune cells and direct visualization of cell infiltration and phagocytic-like behaviors in live animals, we also demonstrate a novel approach to study inter-cellular interactions during glioblastoma initiation, an approach that is not currently feasible in rodent models. In the future, it will be interesting to further assess roles for both the innate and adaptive immune system, as well as associated stroma including endothelial and mesenchymal cells, which can each be effectively studied in our models given the high degree of conservation between zebrafish and human, and the broad availability of validated reporter transgenes.

The contributions of macrophages/microglia to an immunosuppressive TME in glioblastoma and their prevalence within the tumor bulk is well known and has made macrophages an attractive therapeutic target for patients. For example, CSF/CSF-1R interactions have been shown to induce an immunosuppressive M2 phenotype in glioblastoma-associated microglia/macrophages, and blockade of CSF-1R improves survival in tumor burdened mice[16,64]. However, our data and work from others suggests an equally important tumor-suppressive role for microglial/macrophages based on tumor stage and activation state. For example, serial transplantation of transformed mouse neural stem cells results in strong negative pressure from the immune system in syngeneic mice, leading to activation of tumor cell-intrinsic immune evasion mechanisms that support growth *in vivo* and *in vitro*[17]. In addition, recent spatial analyses of human glioblastoma tumor samples identified regions of activated (myeloperoxidase, MPO) macrophages that are associated with improved clinical outcomes, suggesting anti-tumorigenic roles for certain macrophage populations in patients[65]. Our modeling further supports a strong anti-tumor role for pro-inflammatory microglia/macrophages within the endogenous TME at initiation and following transplantation, which is considered an experimental surrogate for relapse potential. Our data also suggests that the pro-tumorigenic immune niche seen in late-stage gliomas is not already established at initiation stages. Given that the transition to mesenchymal-like glioblastoma is closely linked to immune cell infiltration and an immune-suppressive TME[17,66], it will be important to characterize these transitions to better understand anti-tumor mechanisms and their evolution during tumor progression, with the potential for therapeutically harnessing endogenous immune cell types and/or signaling pathways in the future. Altogether, these data suggest an anti-tumor growth but potentially relapse promoting role for therapeutic anti-macrophage approaches, highlighting the importance of future *in vivo* investigations into how inhibition of transitions and/or switching

immunosuppressive microglia/macrophages to immune activating states may inhibit glioblastoma growth or prevent relapse for patients.

Finally, it is well known that the type of glioma affects immune responses, implying that tumor-intrinsic factors shape the composition of the TME[17,66,67]. Therefore, phenotypic differences with respect to glioblastoma-TME interactions in patients and model systems are likely influenced by the genetic background and oncogenic driver events. Human AKT1 over-expression in zebrafish neural cells was previously shown to drive pre-neoplastic lesions in zebrafish larvae and was found to recruit macrophage and microglia populations through the Sdf1b-Cxcr4b signaling pathway[68]. In this model, loss of macrophages resulted in decreased oncogenic proliferation, suggesting tumor-promoting functions for macrophages at initiation stages. In contrast to AKT1 expressing pre-neoplastic neurons, we visualized *mpeg1.1*:GFP+ macrophages/microglia very closely associated with and/or engulfing mScarlet+ p53EPS tumor cellular puncta, suggesting an effort to clear cells and/or cellular debris in p53EPS. This anti-tumor role is further supported by our functional analyses showing increased p53EPS tumor initiation in the context of Irf8 gene knock-out and decreased phagocytic cell development *in vivo* in zebrafish larvae. Given that effectively leveraging targeted therapies for glioblastoma will require a deep and individualized understanding of patient-specific tumor cell biology, in the future it will be important to harness the flexibility of our mosaic oncogene over-expression approach and understand different tumor plus environmental factors in the context of different genetic drivers and/or modifiers identified in patients.

Methods

Zebrafish Husbandry and Care

Animals were raised in accordance with Canadian Council on Animal care (CCAC) guidelines and all experiments were approved under an Animal Use Protocol established with the Animal Care Committee at the Peter Gilgan Centre for Research and Learning (AUP #1000051391 and #1000064586). Previously described zebrafish strains including syngeneic CG1[29], CG1tp53^{del26}, Tg(*mpeg1.1*:EGFP)[43], and Tg(*tnfa*:EGFP)[41] were used as indicated in the manuscript.

Preparation and injection of linearized DNA for tumorigenesis

her4.1:PI3KCA^{H1047R}, *her4.1*:mScarlet, *her4.1*:EGFR^{viii}, *her4.1*:KRAS^{G12D}, *her4.1*:EGFP *her4.1:*Cas9-2A-EGFP, *gfap*:EGFP, and *gfap*:mScarlet transgene expression constructs were cloned using previously described *her4.1* sequence[69] , *gfap* entry plasmid[28], standard Tol2 Gateway plasmids and protocols[70]. *rag2*:EGFP and *mpeg1.1*:EGFP expression plasmids were previously described[43,71]. Circular *her4.1* expression plasmids were linearized using XhoI restriction enzyme (New England Biolabs, R0146S) while *gfap*:EGFP was linearized using ClaI (New England Biolabs, R0197S), according to manufacturer's protocol. Restriction enzymes were heat inactivated and linearized vector purified utilizing an EZ-10 Spin Column PCR Products Purification Kit (Bio Basic, BS364). Injection mixtures such as EPS (*her4.1*:**E**GFR^{viii}, *her4.1*:**P**I3KCA^{H1047R}, *her4.1*:m**S**carlet) or KPG (*her4.1*:**K**RAS, *her4.1*:**P**I3KCA^{H1047R}, *her4.1*:**G**FP) were prepared at 2:1:1 molar ratios in 50% TE Buffer (Invitrogen, 12090-015) with KCl (final concentration 0.1M) and Phenol red (final concentration 5%, Sigma-Aldrich, P0290). CG1 or CG1tp53^{del} embryos were micro injected with 0.5-1nL of injection mixture at the one-cell stage and monitored for tumor development, starting at 10-15 days post fertilization (dpf).

Guide Synthesis and CRISPR-Cas9 Gene Targeting

CRISP/Cas9 sequence targets and guide RNA (gRNA) oligos were designed using CHOPCHOP[72]. Guide RNA were *in vitro* synthesized using the EnGen sgRNA Synthesis Kit (New England Biolabs, E3322V) cording to manufacturer's recommendation.

Cas9 protein with NLS (PNA Bio, CP01-200) was resuspended in 20% glycerol/water to a concentration of 1mg/ml. Cas9/gRNA microinjection mix was prepared at a final concentration of 0.3mg/ml Cas9 + 30-50ng/ul of each gRNA. 0.5-1nL of injection mix and injected into zebrafish embryos of the indicated genotype, at the one-cell stage. CRISPR/Cas9 targeting efficiency was measured following PCR-based locus amplification, Sanger sequencing and Synthego ICE Analysis (ICE analysis, Synthego, ice.synthego.com)[50]. All gRNA sequences and PCR oligos are indicated in Supplementary Table 5.

Brain Dissection and Dissociation

Animals were euthanized with a lethal 300mg/L dose of tricaine (Sigma-Aldrich, E10521) ~10-20 minutes before dissection. Fish were decapitated posterior of the gills and the head transferred to sterile-filtered PBS (Wisent Inc., 311-010-CL). Using fine-tipped forceps, brains were carefully extracted from the skull and transferred to a micro centrifuge tube and kept in PBS at 28°C until further processing. 5-10 brains were transferred to 1ml of 28°C pre-warmed Accutase (Stemcell, 07920), followed by incubation at 28°C with gentle rocking for a total of ~50 minutes. Every 10 minutes, brains were mechanically dissociated with gentle pipetting 15-30 times using a 1mL filter tip. Dissociated tissue were passed through a 40um Cell Strainer (Corning, 352340) into a 50ml conical tube to achieve single cell suspensions. Strained cells were pelleted at approximately 1000 x g for 5 minutes at room temperature and resuspended in PBS.

Bulk Tumor Cell Transplantation

Cell suspensions were maintained at 28°C during the transplantation procedure. 2dpf CG1 syngeneic zebrafish larvae were injected with 1-2nL of cell suspension into the hindbrain ventricle, as previously described[73]. Cells were injected alone or in combination with 1% total volume Clodrosomes (Encapsula Nano Sciences, CLD-8901), vehicle control liposomes, or 0.05ng/nL human CSF-1 recombinant protein (Cell Signaling Technology, 8929SC).

Immunohistochemistry

Zebrafish were fixed overnight in 4% PFA and stored in methanol at -20°C before paraffin embedding and sectioning at the Centre for Chemogenomic Pathology Core Facility. Animal sections were deparaffinized with 2x5 minute washes of Xylenes. Sections were rehydrated with sequential 2x10 minute washes in 100%, 90%, 70% ethanol before sequential rinsing with ddH20, 3% H_2O_2, and ddH20. Slides were then boiled in 1x Citrate Buffer (Sigma-Aldrich, C999) within a standard microwave and rinsed in ddH20, after cooling for 30 minutes. Sections were blocked with TBST/5% Normal Goat Serum for 1 hour at RT before overnight incubation with primary antibody diluted in Diluent CST (Cell Signaling Technology, 8112) at 4°C. The following day slides were washed once with 3x5 minutes with TBS, TBST, and TBS. Samples were then incubated with secondary antibody (Cell Signaling Technology, 8114) for half an hour at room temperature, followed by another 3x5 minute TBS/T wash. Standard DAB development (Thermo Scientific, 34002) was performed for 5-7 minutes, followed by water termination. Samples were Hematoxylin (VWR, 10143-146) stained with a 1:6 diluted solution for 3-5 seconds and rinsed 5x with tap water. Slides were dehydrated sequentially with 70%, 90%, 100% ethanol washes followed by 2x5 minute Xylene washes before being mounted with glass cover slips and Permount (Fisher Scientific, SP15-100). Primary antibodies raised against proliferating cell

nuclear antigen (PCNA, Cell Signaling, D3H8P), phosphorylated ERK (Cell Signaling, #9101) and phosphorylated AKT (Cell Signaling, #9271) were used.

Bulk RNASeq Library Preparation, Quantification and Differential Gene Expression Analysis

Three p53KPG, p53EPS, and control-injected brains (from non-tumor forming injected siblings) were harvested at 20-30 dpf and immediately placed into 1mL of TRIzol Reagent (Invitrogen, 15596026). mScarlet+ tumor cells were also sorted from bulk (non-fluorescent) tissue from pooled brains at the SickKids-UHN Flow Cytometry Core Facility on a Sony MA900 VBYR cell sorter, before pelleting and lysis in TRIzol Reagent. Total RNA was purified for all samples using a Monarch RNA Cleanup Kit (New England Biolabs, T2040L), according to manufacturer's recommendations. Sequence ready polyA-enriched libraries were prepared using the NEB Ultra II Directional mRNA prep kit for Illumina (NEB, E7760), according to manufacturer's recommendations. Single-end 150bp sequencing at a targeted depth of ~30-60 million reads/sample was performed using an Illumina NovaSeq S1 flowcell, at the Centre for Applied Genomics (TCAG). Raw .fastq data was processed using Salmon quantification of transcripts for each sample. A "decoy-aware" index was built with the *Danio rerio* transcriptome and genome using the GRCz11 assembly with a k-mers length of 23. Samples were then quantified with the following arguments: -r, --seqBias, --mp -3, --validateMappings, --rangeFactorizationBins 4.

Human Ortholog Conversion and GSEA

Normalized counts output from DESeq2 for the above processed data were utilized for GSEA analysis without any further trimming or processing, as recommend by the GSEA user

guide[30,31]. Zebrafish transcripts were assigned known or high-confidence Human orthologs using Ensembl BioMart, as previously described[74]. Bulk sequencing data from *her4.1:*KRAS^{G12D} or *her4.1:*EGFR^{viii} driven tumors, or sorted cells derived from such, were compared with non-tumour control brains under default conditions (1000 permutations, gene set). Expression signatures were compared against published glioblastoma[6,19], medulloblastoma[32], or Hallmark gene sets[33], as indicated in the manuscript.

Neutral Red Staining and Quantification

Zebrafish were treated with Neutral Red, as previously described[75]. Animals were then anesthetized in Tricaine and oriented on their sides in 3% methylcellulose before an image stack of approximately 120-150um depth was taken beginning from the surface of the otic vesicle into the fish. Neutral Red stained foci were counted using Zen Lite Software (version 3.3) in an area bounded by the posterior edge of the eye and the posterior edge of the otic vesicle for each fish.

Image Acquisition

Flourescence and bright field image acquisition of whole animals and dissected tumor-burdened brains was performed using a Zeiss Axiozoom V16 macroscope. High resolution confocal microscopy was performed using a Nikon 1AR confocal microscope, with image processing and Z-stack compression performed using ImageJ software.

RT-qPCR and Analysis

Total RNA was extracted from tumor-burdened brains using TRIzol reagent, as described above, and reverse transcribed using the High-Capacity DNA Reverse Transcriptase Kit

(Thermo Fisher, 4368814), as per manufacturer's recommendations. RT-qPCR was performed using the SYBR Green I Master kit (Roche, 04887352001) following the manufacturer's recommended protocol and a Bio-Rad CFX96 qPCR Real-Time PCR Module with C1000 Touch Termal Cycler Unit. All primers used to amplify genes of interest are indicated in Supplementary Table 5. At least 5 brain samples were pooled for each sample, with gene expression normalized to *18s*. Where indicated, gene expression was normalized to *mScarlet* expression to control for differences in overall tumor size.

Acknowledgements: We thank Dr. David Langenau for CG1*tp53*^{del} zebrafish. We also thank the Centre for Phenogenomics (TCP) Histopathology core for tissue processing and staining, the Centre for Applied Genomics (TCAG) for sequencing, the SickKids Imaging Facility, and the Zebrafish Genetics and Disease Models Facility management and support team for zebrafish husbandry.

Financial Support: This project was funded by the Canadian Institutes of Health Research.

References

1. Ostrom, Q. T. *et al.* CBTRUS Statistical Report: Primary brain and other central nervous system tumors diagnosed in the United States in 2010-2014. *Neuro Oncol* **19**, v1–v88 (2017).
2. Torp, S. H., Solheim, O. & Skjulsvik, A. J. The WHO 2021 Classification of Central Nervous System tumours: a practical update on what neurosurgeons need to know—a minireview. *Acta Neurochir (Wien)* **164**, 2453–2464 (2022).
3. Aldape, K. *et al.* Challenges to curing primary brain tumours. *Nat Rev Clin Oncol* **16**, 509–520 (2019).
4. Brennan, C. W. *et al.* The somatic genomic landscape of glioblastoma. *Cell* **155**, 462 (2013).
5. Verhaak, R. G. W. *et al.* Integrated Genomic Analysis Identifies Clinically Relevant Subtypes of Glioblastoma Characterized by Abnormalities in PDGFRA, IDH1, EGFR, and NF1. *Cancer Cell* **17**, 98–110 (2010).
6. Wang, Q. *et al.* Tumor Evolution of Glioma-Intrinsic Gene Expression Subtypes Associates with Immunological Changes in the Microenvironment. *Cancer Cell* **32**, 42-56.e6 (2017).
7. Phillips, H. S. *et al.* Molecular subclasses of high-grade glioma predict prognosis, delineate a pattern of disease progression, and resemble stages in neurogenesis. *Cancer Cell* **9**, 157–173 (2006).
8. Neftel, C. *et al.* An Integrative Model of Cellular States, Plasticity, and Genetics for Glioblastoma. *Cell* **178**, 835-849.e21 (2019).
9. Patel, A. P. *et al.* Single-cell RNA-seq highlights intratumoral heterogeneity in primary glioblastoma. *Science (1979)* **344**, 1396–1401 (2014).
10. Darmanis, S. *et al.* Single-Cell RNA-Seq Analysis of Infiltrating Neoplastic Cells at the Migrating Front of Human Glioblastoma. *Cell Rep* **21**, 1399–1410 (2017).
11. Bikfalvi, A. *et al.* Challenges in glioblastoma research: focus on the tumor microenvironment. *Trends in Cancer* vol. 9 9–27 Preprint at https://doi.org/10.1016/j.trecan.2022.09.005 (2023).
12. Quail, D. F. & Joyce, J. A. The Microenvironmental Landscape of Brain Tumors. *Cancer Cell* vol. 31 326–341 Preprint at https://doi.org/10.1016/j.ccell.2017.02.009 (2017).
13. McGranahan, T., Therkelsen, K. E., Ahmad, S. & Nagpal, S. Current State of Immunotherapy for Treatment of Glioblastoma. *Current Treatment Options in Oncology* vol. 20 Preprint at https://doi.org/10.1007/s11864-019-0619-4 (2019).

14. Sengupta, S., Marrinan, J., Frishman, C. & Sampath, P. Impact of temozolomide on immune response during malignant glioma chemotherapy. *Clinical and Developmental Immunology* vol. 2012 Preprint at https://doi.org/10.1155/2012/831090 (2012).
15. Pearson, J. R. D. *et al.* Immune Escape in Glioblastoma Multiforme and the Adaptation of Immunotherapies for Treatment. *Frontiers in Immunology* vol. 11 Preprint at https://doi.org/10.3389/fimmu.2020.582106 (2020).
16. Kennedy, B. C. *et al.* Tumor-associated macrophages in glioma: Friend or foe? *Journal of Oncology* Preprint at https://doi.org/10.1155/2013/486912 (2013).
17. Gangoso, E. *et al.* Glioblastomas acquire myeloid-affiliated transcriptional programs via epigenetic immunoediting to elicit immune evasion. *Cell* **184**, 2454-2470.e26 (2021).
18. Parmigiani, E. *et al.* Interferon-γ resistance and immune evasion in glioma develop via Notch-regulated co-evolution of malignant and immune cells. *Dev Cell* **57**, 1847-1865.e9 (2022).
19. McLendon, R. *et al.* Comprehensive genomic characterization defines human glioblastoma genes and core pathways. *Nature* **455**, 1061–1068 (2008).
20. Zhang, Y. *et al.* The p53 pathway in glioblastoma. *Cancers (Basel)* **10**, (2018).
21. Takke, C., Dornseifer, P., Weizsäcker, E. V. & Campos-Ortega, J. A. her4, a zebrafish homologue of the Drosophila neurogenic gene E(spl), is a target of NOTCH signalling. *Development* **126**, 1811–1821 (1999).
22. Chen, X. *et al.* A Feedforward Mechanism Mediated by Mechanosensitive Ion Channel PIEZO1 and Tissue Mechanics Promotes Glioma Aggression. *Neuron* **100**, 799-815.e7 (2018).
23. Holland, J. D., Klaus, A., Garratt, A. N. & Birchmeier, W. Wnt signaling in stem and cancer stem cells. *Curr Opin Cell Biol* **25**, 254–264 (2013).
24. Haddad, A. F. *et al.* Mouse models of glioblastoma for the evaluation of novel therapeutic strategies. *Neurooncol Adv* **3**, 1–16 (2021).
25. Than-Trong, E. *et al.* Lineage hierarchies and stochasticity ensure the long-term maintenance of adult neural stem cells. *Sci Adv* **6**, 26–29 (2020).
26. Ignatius, M. S. *et al.* Tp53 deficiency causes a wide tumor spectrum and increases embryonal rhabdomyosarcoma metastasis in zebrafish. *Elife* **7**, e37202 (2018).
27. Langenau, D. M. *et al.* Co-injection strategies to modify radiation sensitivity and tumor initiation in transgenic Zebrafish. *Oncogene* **27**, 4242–4248 (2008).
28. Don, E. K. *et al.* A Tol2 Gateway-Compatible Toolbox for the Study of the Nervous System and Neurodegenerative Disease. *Zebrafish* **14**, 69–72 (2017).
29. Mizgireuv, I. V. & Revskoy, S. Y. Transplantable tumor lines generated in clonal zebrafish. *Cancer Res* **66**, 3120–3125 (2006).

30. Mootha, V. K. *et al.* PGC-1α-responsive genes involved in oxidative phosphorylation are coordinately downregulated in human diabetes. *Nat Genet* (2003) doi:10.1038/ng1180.
31. Subramanian, A. *et al.* Gene set enrichment analysis: A knowledge-based approach for interpreting genome-wide expression profiles. *Proceedings of the National Academy of Sciences* (2005) doi:10.1073/pnas.0506580102.
32. Cavalli, F. M. G. *et al.* Intertumoral Heterogeneity within Medulloblastoma Subgroups. *Cancer Cell* **31**, 737-754.e6 (2017).
33. Liberzon, A. *et al.* Molecular signatures database (MSigDB) 3.0. *Bioinformatics* **27**, 1739–1740 (2011).
34. Park, J. H. & Lee, H. K. Current Understanding of Hypoxia in Glioblastoma Multiforme and Its Response to Immunotherapy. *Cancers* vol. 14 Preprint at https://doi.org/10.3390/cancers14051176 (2022).
35. Majc, B. *et al.* Epithelial-to-mesenchymal transition as the driver of changing carcinoma and glioblastoma microenvironment. *Biochimica et Biophysica Acta - Molecular Cell Research* vol. 1867 Preprint at https://doi.org/10.1016/j.bbamcr.2020.118782 (2020).
36. Yang, K. *et al.* Identification of a unique tumor cell subset employing myeloid transcriptional circuits to create an immunomodulatory microenvironment in glioblastoma. *Oncoimmunology* **11**, 1–15 (2022).
37. Khan, F. *et al.* Macrophages and microglia in glioblastoma: heterogeneity, plasticity, and therapy. *Journal of Clinical Investigation* vol. 133 Preprint at https://doi.org/10.1172/JCI163446 (2023).
38. Gutmann, D. H. & Kettenmann, H. Microglia/Brain Macrophages as Central Drivers of Brain Tumor Pathobiology. *Neuron* vol. 104 442–449 Preprint at https://doi.org/10.1016/j.neuron.2019.08.028 (2019).
39. Herbomel, P., Thisse, B. & Thisse, C. Zebrafish early macrophages colonize cephalic mesenchyme and developing brain, retina, and epidermis through a M-CSF receptor-dependent invasive process. *Dev Biol* **238**, 274–288 (2001).
40. Shiau, C. E., Kaufman, Z., Meireles, A. M. & Talbot, W. S. Differential requirement for irf8 in formation of embryonic and adult macrophages in zebrafish. *PLoS One* **10**, 1–15 (2015).
41. Nguyen-Chi, M. *et al.* Identification of polarized macrophage subsets in zebrafish. *Elife* **4**, 1–14 (2015).
42. Hao, N. B. *et al.* Macrophages in tumor microenvironments and the progression of tumors. *Clin Dev Immunol* **2012**, (2012).

43. Ellett, F., Pase, L., Hayman, J. W., Andrianopoulos, A. & Lieschke, G. J. Mpeg1 Promoter Transgenes Direct Macrophage-Lineage Expression in Zebrafish. *Blood* **117**, 49–56 (2011).
44. Nimmerjahn A, Kirchhoff F & Helmchen F. Resting Microglial Cells Are Highly Dynamic Surveillants of Brain Parenchyma in Vivo. *Science (1979)* **308**, 1314–1318 (2005).
45. Karperien, A., Ahammer, H. & Jelinek, H. F. Quantitating the subtleties of microglial morphology with fractal analysis. *Frontiers in Cellular Neuroscience* 1–34 Preprint at https://doi.org/10.3389/fncel.2013.00003 (2013).
46. Ning, S., Pagano, J. S. & Barber, G. N. IRF7: Activation, regulation, modification and function. *Genes Immun* **12**, 399–414 (2011).
47. Günthner, R. & Anders, H. J. Interferon-regulatory factors determine macrophage phenotype polarization. *Mediators Inflamm* **2013**, (2013).
48. Feng, H. *et al.* Zebrafish IRF1, IRF3, and IRF7 Differentially Regulate IFNΦ1 and IFNΦ3 Expression through Assembly of Homo- or Heteroprotein Complexes. *The Journal of Immunology* **197**, 1893–1904 (2016).
49. Hu, S. Q. *et al.* Interferon regulatory factor-7 is required for hair cell development during zebrafish embryogenesis. *Dev Neurobiol* **82**, 88–97 (2022).
50. Synthego. Synthego Performance Analysis, ICE Analysis. Preprint at (2019).
51. Yang, K. *et al.* Identification of a unique tumor cell subset employing myeloid transcriptional circuits to create an immunomodulatory microenvironment in glioblastoma. *Oncoimmunology* **11**, (2022).
52. Jin, X. *et al.* Interferon regulatory factor 7 regulates glioma stem cells via interleukin-6 and Notch signalling. *Brain* **135**, 1055–1069 (2012).
53. Hanlon, L. A., Raghupathi, R. & Huh, J. W. Depletion of microglia immediately following traumatic brain injury in the pediatric rat: Implications for cellular and behavioral pathology. *Exp Neurol* **316**, 39–51 (2019).
54. Yang, L., Rojas, A. M. & Shiau, C. E. Liposomal clodronate-mediated macrophage depletion in the zebrafish model. *Bio Protoc* **11**, (2021).
55. Yan, C. *et al.* Visualizing Engrafted Human Cancer and Therapy Responses in Immunodeficient Zebrafish. *Cell* **177**, 1903–1914 (2019).
56. Wu, S. *et al.* Il34-Csf1r Pathway Regulates the Migration and Colonization of Microglial Precursors. *Dev Cell* **46**, 552-563.e4 (2018).
57. Herbomel, P., Thisse, B. & Thisse, C. Zebrafish early macrophages colonize cephalic mesenchyme and developing brain, retina, and epidermis through a M-CSF receptor-dependent invasive process. *Dev Biol* **238**, 274–288 (2001).

58. Gómez-Oliva, R. *et al.* Evolution of Experimental Models in the Study of Glioblastoma: Toward Finding Efficient Treatments. *Frontiers in Oncology* vol. 10 Preprint at https://doi.org/10.3389/fonc.2020.614295 (2021).
59. Haddad, A. F. *et al.* Mouse models of glioblastoma for the evaluation of novel therapeutic strategies. *Neuro-Oncology Advances* vol. 3 Preprint at https://doi.org/10.1093/noajnl/vdab100 (2021).
60. Mayrhofer, M. *et al.* A novel brain tumour model in zebrafish reveals the role of YAP activation in MAPK- and PI3K-induced malignant growth. *DMM Disease Models and Mechanisms* **10**, 15–28 (2017).
61. Ju, B. *et al.* Oncogenic KRAS promotes malignant brain tumors in zebrafish. *Mol Cancer* **14**, (2015).
62. Almstedt, E. *et al.* Real-time evaluation of glioblastoma growth in patient-specific zebrafish xenografts. *Neuro Oncol* **24**, 726–738 (2022).
63. Modzelewska, K. *et al.* MEK Inhibitors Reverse Growth of Embryonal Brain Tumors Derived from Oligoneural Precursor Cells. *Cell Rep* **17**, 1255–1264 (2016).
64. Pyonteck, S. M. *et al.* CSF-1R inhibition alters macrophage polarization and blocks glioma progression. *Nat Med* **19**, 1264–1272 (2013).
65. Karimi, E. *et al.* Single-cell spatial immune landscapes of primary and metastatic brain tumours. *Nature* **614**, 555–563 (2023).
66. Klemm, F. *et al.* Interrogation of the Microenvironmental Landscape in Brain Tumors Reveals Disease-Specific Alterations of Immune Cells. *Cell* **181**, 1643-1660.e17 (2020).
67. Friebel, E. *et al.* Single-Cell Mapping of Human Brain Cancer Reveals Tumor-Specific Instruction of Tissue-Invading Leukocytes. *Cell* **181**, 1626-1642.e20 (2020).
68. Chia, K., Mazzolini, J., Mione, M. & Sieger, D. Tumor initiating cells induce Cxcr4-mediated infiltration of pro-tumoral macrophages into the brain. doi:10.7554/eLife.31918.001.
69. Yeo, S. Y., Kim, M. J., Kim, H. S., Huh, T. L. & Chitnis, A. B. Fluorescent protein expression driven by her4 regulatory elements reveals the spatiotemporal pattern of Notch signaling in the nervous system of zebrafish embryos. *Dev Biol* **301**, 555–567 (2007).
70. Kwan, K. M. *et al.* The Tol2kit: A multisite gateway-based construction Kit for Tol2 transposon transgenesis constructs. *Developmental Dynamics* **236**, 3088–3099 (2007).
71. Langenau, D. M. *et al.* Effects of RAS on the genesis of embryonal rhabdomyosarcoma. *Genes Dev* **21**, 1382–95 (2007).
72. Labun, K. *et al.* CHOPCHOP v3: Expanding the CRISPR web toolbox beyond genome editing. *Nucleic Acids Res* **47**, W171–W174 (2019).

73. Casey, M. J. *et al.* Transplantation of Zebrafish pediatric brain tumors into immune-competent hosts for long-term study of tumor cell behavior and drug response. *Journal of Visualized Experiments* **2017**, (2017).
74. Demirci, Y. *et al.* Brain Regeneration Resembles Brain Cancer at Its Early Wound Healing Stage and Diverges From Cancer Later at Its Proliferation and Differentiation Stages. *Front Cell Dev Biol* **10**, (2022).
75. Shiau, C. E., Monk, K. R., Joo, W. & Talbot, W. S. An anti-inflammatory nod-like receptor is required for microglia development. *Cell Rep* **5**, 1342–1352 (2013).

Figure Legends

Figure 1. *her4.1*-driven over-expression of patient-relevant oncogenes drives glial-derived brain tumor formation in syngeneic *tp53* loss-of-function mutant zebrafish. (A) Schematic of modeling strategy where linearized transgene vectors with the zebrafish *her4.1* promoter driving human EGFR^{viii}, human PI3KCA^{H1047R}, and mScarlet fluorescent protein are co-injected at the one-cell stage into syngeneic (CG1) *tp53*$^{-/-}$ mutant zebrafish embryos. Starting at 15 days post fertilization (dpf), mosaic-injected zebrafish are screened for CNS tumor formation, indicated by mScarlet expression in the brain region of live zebrafish. Co-injection of *gfap:*GFP linearized transgene is used to assess glial-specific cell fate specification *in vivo*. **(B)** *her4.1:*mScarlet and *gfap:*GFP expression in the anterior CNS of mosaic-injected syngeneic (CG1) *tp53*$^{-/-}$ zebrafish at 30dpf. **(C)** Whole brain dissected from a p53EPS mosaic-injected zebrafish at 30dpf. **(D)** Cumulative frequencies of mScarlet+ CNS lesions in syngeneic *tp53*$^{-/-}$ mutant (CG1*tp53*$^{-/-}$) and wild-type (CG1) zebrafish injected at the one cell stage with *her4.1:*EGFR^{viii} (E), *her4.1:*PI3KCA^{H1047R} (P), and/or *her4.1:*mScarlet (S). **(E)** Syngeneic (CG1) zebrafish at 30dpf engrafted with *her4.1:*mScarlet+/*gfap:*GFP+ brain tumor cells, following primary transplantation (1T) at 2dpf into the embryonic brain ventricle. **(F)** Whole brain dissected from engrafted syngeneic host (CG1) zebrafish at 30dpf. **(G)** FACS plot of bulk syngeneic host brain following primary transplant (1T) of *her4.1:*EGFR^{viii} + *her4.1:*PI3KCA^{H1047R} + *her4.1:*mScarlet + *gfap:*GFP brain tumor cells. **(H)** Hematoxylin and eosin (H&E) staining of brain region of p53EPS mosaic-injected zebrafish at 30dpf. Inset highlights tumor region. Scale bars represent 200μm and 20μm, respectively. **(I-K)** Immunohistochemical staining of proliferating cell nuclear antigen (PCNA, I), phosphorylated ERK (p-ERK, J), and phosphorylated AKT (p-AKT, K) on tumor section. Scare bars represent 50μm.

Figure 2. RNA expression analysis establishes enrichment of mesenchymal glioblastoma and inflammation signatures in p53EPS model. (A) Principal component analysis (PCA) of mRNA sequencing from whole control injected brains (CTRL), p53EPS and p53KPS tumor-burdened brains. **(B)** Heatmap of normalized counts for genes upregulated in p53EPS tumor-burdened brains (log2FoldChange > 2, padj < 0.05), compared to whole control injected brains (CTRL). A selected list of upregulated transcripts is indicated. **(C)** Gene set enrichment analysis (GSEA) plots of published gene signatures for mesenchymal subtype glioblastoma for genes differentially regulated in p53EPS compared to control injected brains[6,19]. Normalized Enrichment Scores (NES) and False Discovery Rates (FDR) are indicated. **(D)** Bar plot of Normalized Enrichment Score from Gene Set Enrichment Analysis (GSEA) of Hallmark gene sets[33]. **(E)** Volcano plots of differentially expressed genes between sorted mScarlet+ p53EPS tumor cells and control injected whole brain tissue (CTRL WB), and sorted mScarlet-negative cells from p53EPS tumor-burdened brains and control injected whole brains (CTRL WB). **(F)** *her4.1:*mScarlet and *rag2:*EGFP expression in live zebrafish with a p53EPS tumor at 30 dpf. **(G)** FACS plot of p53EPS brain with *rag2*:EGFP co-expression from (F). **(H, I)** *her4.1:*mScarlet and *mpeg1.1:*EGFP expression in live zebrafish with a p53EPS tumor at 30 dpf.

Figure 3. p53EPS recruits activated microglia/macrophages at early stages of tumor initiation. (A) Neutral red staining of mScarlet-negative and mScarlet+ p53EPS injected brains at 10 dpf. Neutral red foci in early-stage lesions are highlighted with arrows and are indicative of phagocytic cells. **(B)** Whole brain with p53EPS-induced tumor in a transgenic Tg(*tnfa:*EGFP) zebrafish at 20 dpf. Black arrows indicate *tnfa:*EGFP+ punctae associated with mScarlet+ brain tumor lesion. **(C)** Z-stack projections of three independent p53EPS brains at 10-13 dpf in

transgenic Tg(*mpeg1.1*:GFP) background. **(D)** Quantification of tumor-associated *mpeg1.1*:GFP+ cells with overlapping and/or internalized *her4.1:*mScarlet+ punctae (n=3).

Figure 4. Inflammation-associated *irf7* and *irf8* inhibit p53EPS formation *in vivo*. (A-C) Primary (1°) control (A), *irf7* CRISPR/Cas9 (B), and *irf8* CRISPR/Cas9 (C) injected p53EPS at 30 dpf. **(D)** p53EPS incidence at 30 dpf in control (n=3 independent experiments, 108 zebrafish), *irf7* CRISPR/Cas9 (***p<0.0001, Fisher's exact test, n=2 independent experiments, 31 zebrafish), and *irf8* CRISPR/Cas9 (*p=0.0155, Fisher's exact test, n= 2 independent experiments, 36 total injected zebrafish). **(E)** Tg(*her4.1*:Cas9-2A-EGFP) expression at 30 dpf. **(F)** mScarlet+ p53EPS at 30 dpf in Tg(*her4.1*:Cas9-2A-EGFP) injected with *irf7* gRNAs at the one-cell stage. **(G)** p53EPS incidence at 30 dpf in Tg(*her4.1*:Cas9-2A-EGFP)-negative gRNA-injected control siblings, and Tg(*her4.1*:Cas9-2A-EGFP) zebrafish injected at the one-cell stage with *irf7* or *irf8* gRNAs. n.s. not significant, Fisher's exact test.

Figure 5. Inflammation-associated microglia/macrophages inhibit p53EPS tumor engraftment. (A,B) CG1 syngeneic host zebrafish at 20 dpf engrafted with p53EPS tumor cells transplanted with vehicle control (A) or Clodronate liposomes (B) at 2 dpf. **(C-E)** Quantification of p53EPS control engrafted and p53EPS tumors engrafted into CG1 host embryos with (C) Clodronate liposomes (p=0.0048, Fisher's exact test, n=2 independent experiments, total 56 transplanted vehicle control and 50 transplanted Clodrosome-injected hosts), (D) engrafted into *irf8* CRISPR/Cas9-injected into CG1 syngeneic host embryos (p=0.0002, Fisher's exact test, n=2 independent experiments, total 100 transplanted control and 74 transplanted *irf8* CRISPR/Cas9-injected hosts).

Figures

Figure 1

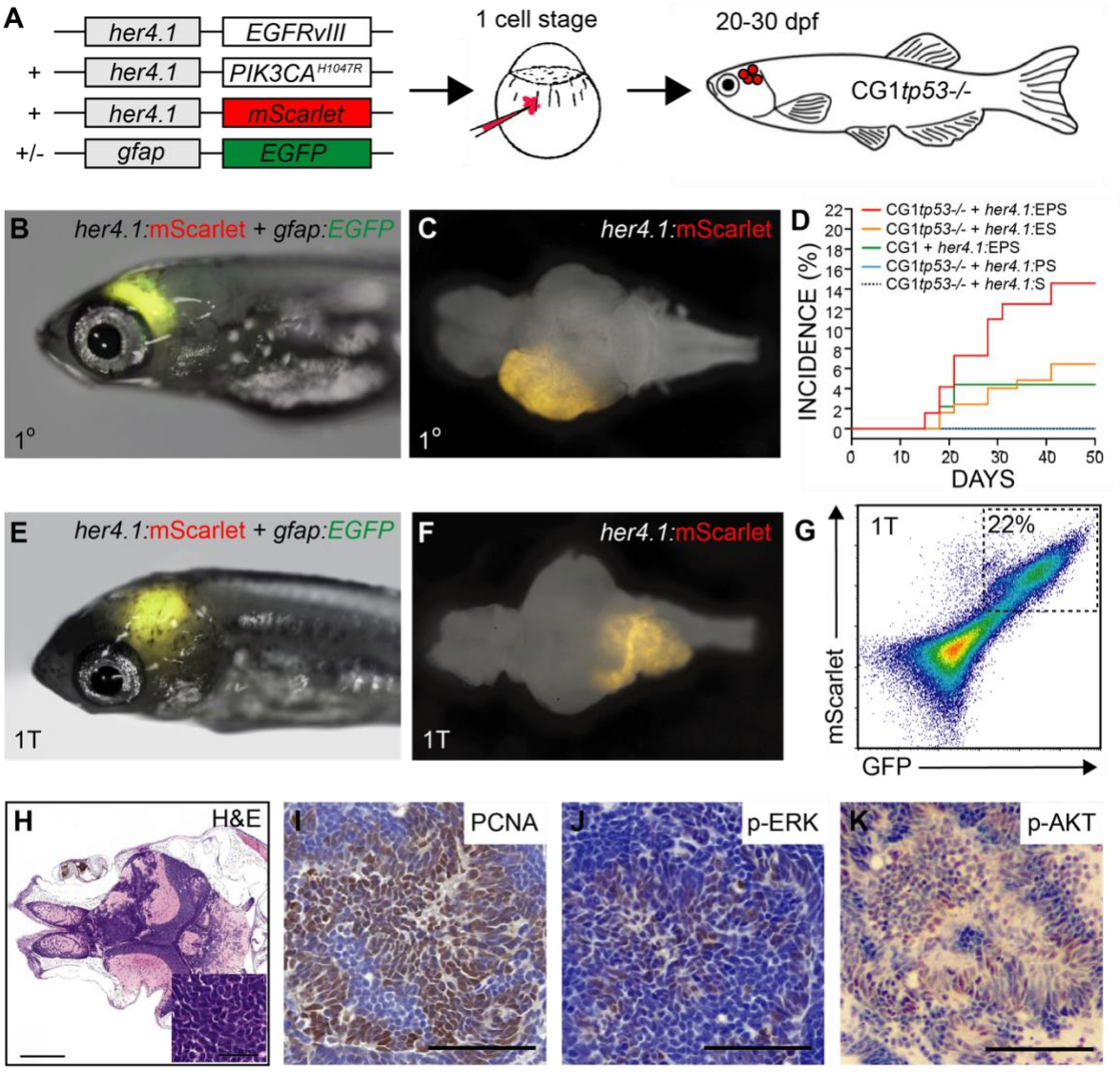

Figure 2

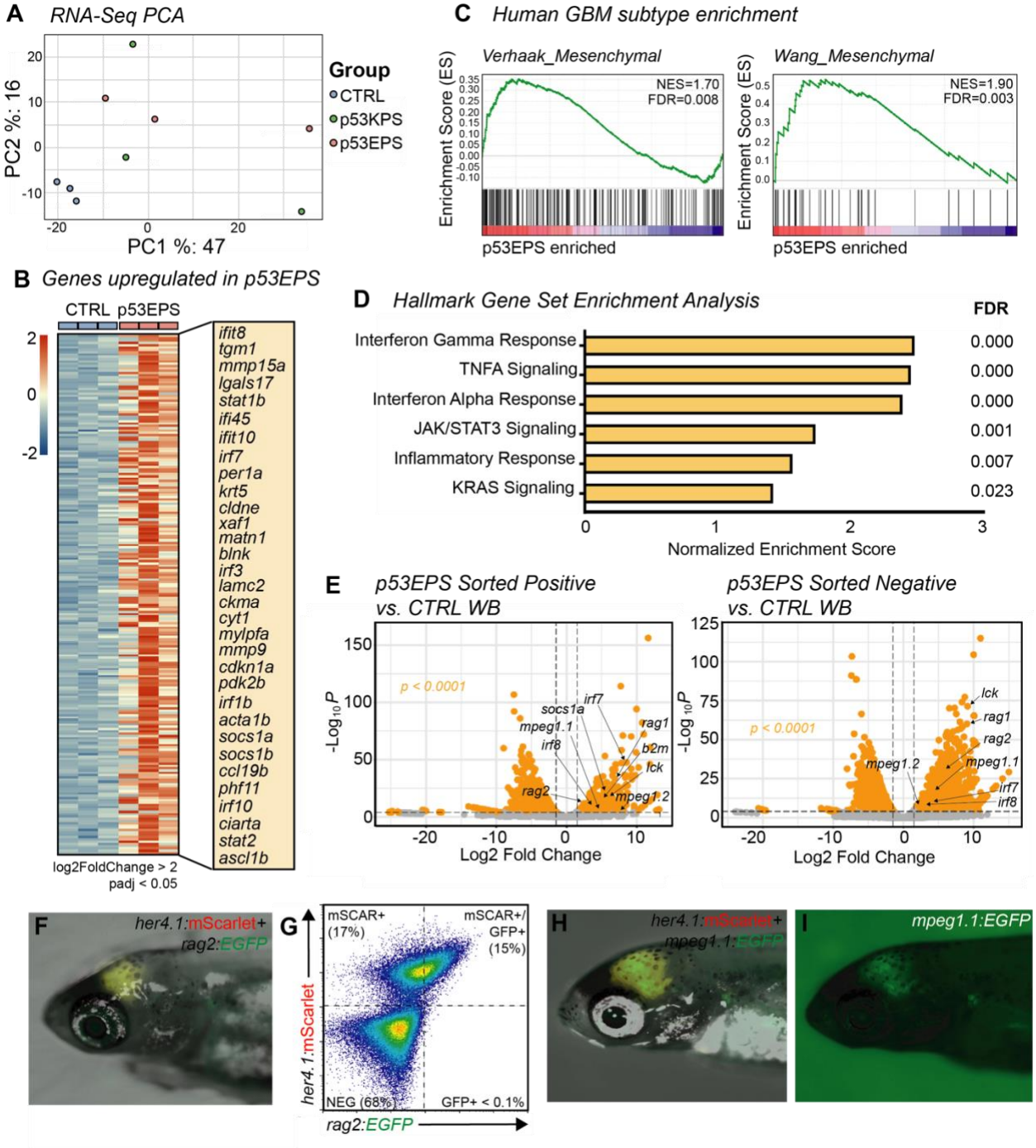
A RNA-Seq PCA
PC2 %: 16
PC1 %: 47
Group
CTRL
p53KPS
p53EPS
B Genes upregulated in p53EPS
CTRL p53EPS
ifit8
tgm1
mmp15a
lgals17
stat1b
ifi45
ifit10
irf7
per1a
krt5
cldne
xaf1
matn1
blnk
irf3
lamc2
ckma
cyt1
mylpfa
mmp9
cdkn1a
pdk2b
irf1b
acta1b
socs1a
socs1b
ccl19b
phf11
irf10
ciarta
stat2
ascl1b
log2FoldChange > 2
padj < 0.05
C Human GBM subtype enrichment
Verhaak_Mesenchymal
NES=1.70
FDR=0.008
Wang_Mesenchymal
NES=1.90
FDR=0.003
Enrichment Score (ES)
p53EPS enriched
D Hallmark Gene Set Enrichment Analysis
FDR
Interferon Gamma Response 0.000
TNFA Signaling 0.000
Interferon Alpha Response 0.000
JAK/STAT3 Signaling 0.001
Inflammatory Response 0.007
KRAS Signaling 0.023
Normalized Enrichment Score
E p53EPS Sorted Positive vs. CTRL WB
p53EPS Sorted Negative vs. CTRL WB
p < 0.0001
socs1a
irf7
mpeg1.1
irf8
rag1
b2m
lck
rag2
mpeg1.2
-Log10P
Log2 Fold Change
F her4.1:mScarlet+ rag2:EGFP
G mSCAR+ (17%)
mSCAR+/ GFP+ (15%)
NEG (68%)
GFP+ < 0.1%
her4.1:mScarlet
rag2:EGFP
H her4.1:mScarlet+ mpeg1.1:EGFP
I mpeg1.1:EGFP

Figure 3

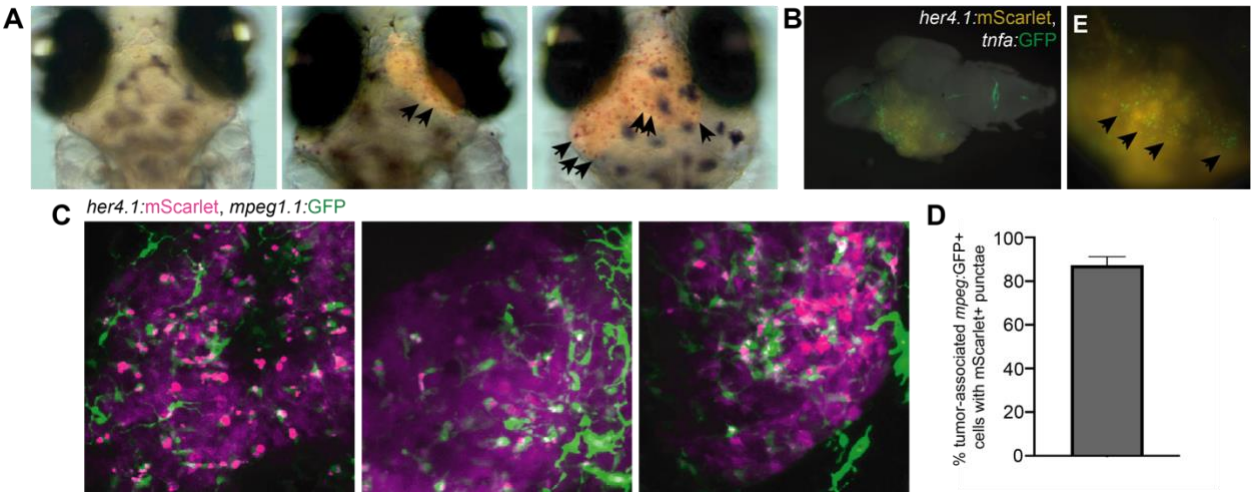
A
B
her4.1:mScarlet,
tnfa:GFP
E
C
her4.1:mScarlet, mpeg1.1:GFP
D
% tumor-associated mpeg:GFP+
cells with mScarlet+ punctae
100
80
60
40
20
0

Figure 4

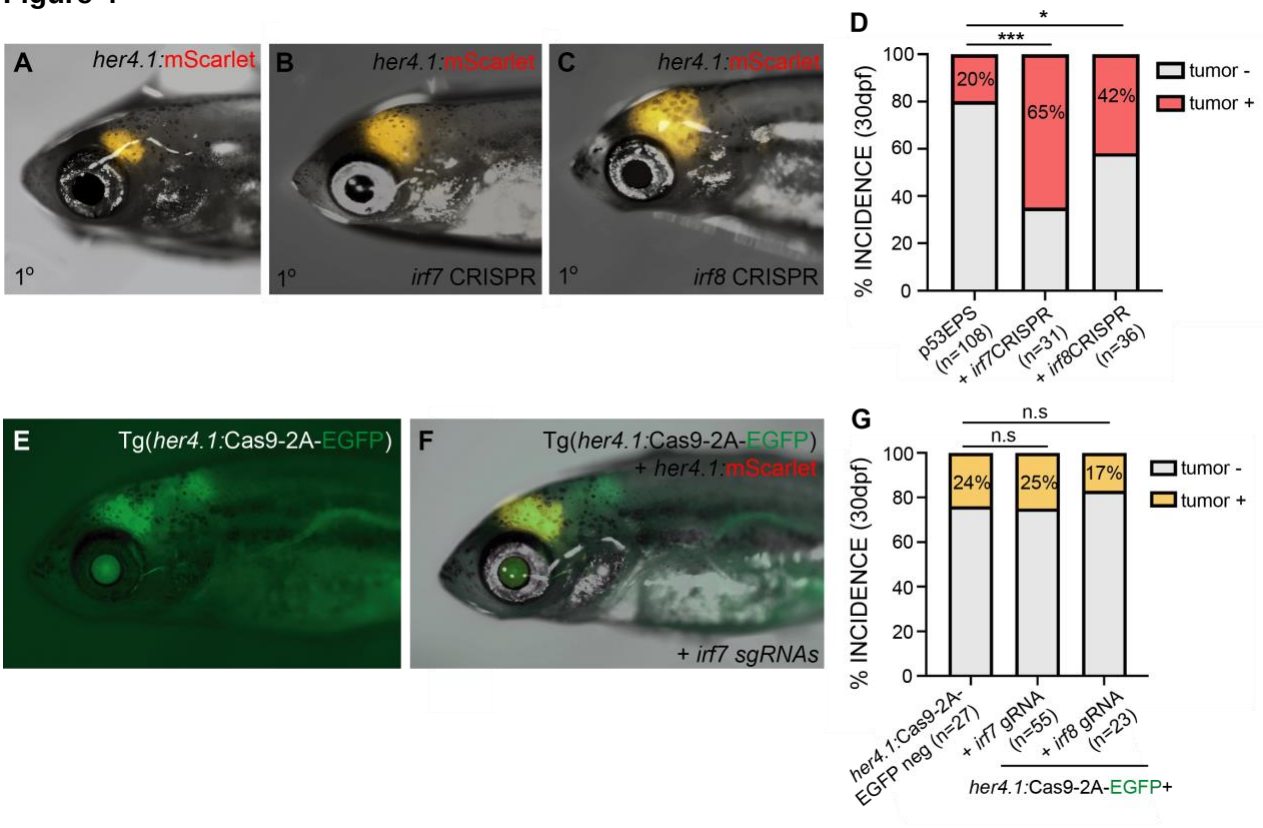
A
her4.1:mScarlet
1°
B
her4.1:mScarlet
1°
irf7 CRISPR
C
her4.1:mScarlet
1°
irf8 CRISPR
D
*
***
% INCIDENCE (30dpf)
100
80
60
40
20
0
20%
65%
42%
tumor -
tumor +
p53EPS (n=108)
+ irf7CRISPR (n=31)
+ irf8CRISPR (n=36)
E
Tg(her4.1:Cas9-2A-EGFP)
F
Tg(her4.1:Cas9-2A-EGFP)
+ her4.1:mScarlet
+ irf7 sgRNAs
G
n.s
n.s
% INCIDENCE (30dpf)
100
80
60
40
20
0
24%
25%
17%
tumor -
tumor +
her4.1:Cas9-2A-EGFP neg (n=27)
+ irf7 gRNA (n=55)
+ irf8 gRNA (n=23)
her4.1:Cas9-2A-EGFP+

Figure 5

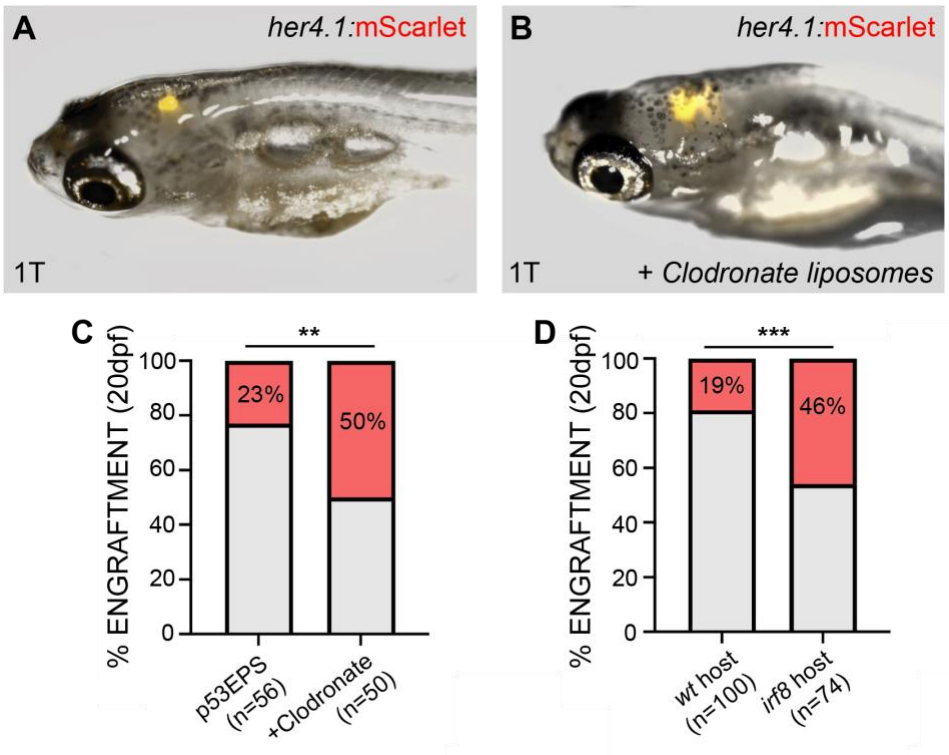
A
her4.1:mScarlet
1T
B
her4.1:mScarlet
1T
+ Clodronate liposomes
C
% ENGRAFTMENT (20dpf)
**
23%
50%
p53EPS (n=56)
+Clodronate (n=50)
D
% ENGRAFTMENT (20dpf)
***
19%
46%
wt host (n=100)
irf8 host (n=74)

Supplementary Figures

Supplementary Figure 1. Inter-tumoral heterogeneity in p53EPS induced tumors. Sample screens of p53EPS injected fish from three different cohorts showing distinct tumor initiation sites and varying degrees of mScarlet-fluorescent intensity, with intense fluorescence indicative of tumorigenesis. Tumors predominantly arise in the optic tectum/mesencephalon region (21/29) with a distinctive subset appearing in the telencephalon/diencephalon region (8/29). Distinct tumors did not arise in the cerebellum/rhombencephalon regions over the course of our experiments.

Supplementary Figure 2. (A) *her4.1:*mScarlet and *gfap:*GFP expression in the anterior CNS of 30dpf syngeneic (CG1) *tp53*$^{-/-}$ zebrafish injected at the one-cell stage with linearized *her4.1:*KRAS^{G12D} + *her4.1:*PI3KCA^{H1047R} + *her4.1:*GFP + *gfap:*mScarlet transgenes. **(B)** Whole brain dissected from mosaic-injected *her4.1:*KRAS^{G12D} + *her4.1:*PI3KCA^{H1047R} + *her4.1:*GFP zebrafish at 30dpf. **(C)** Cumulative frequencies of GFP+ brain lesions in syngeneic *tp53*$^{-/-}$ mutant (CG1*tp53*$^{-/-}$) and wild-type (CG1) zebrafish injected at the one cell stage with *her4.1:*KRAS^{G12D} (K), *her4.1:*PI3KCA^{H1047R} (P), and/or *her4.1:*GFP (G). **(D)** Immunohistochemical staining of proliferating cell nuclear antigen (PCNA), phosphorylated ERK (p-ERK), and phosphorylated AKT (p-AKT) on *her4.1:*KRAS^{G12D} + *her4.1:*PI3KCA^{H1047R} + *her4.1:*GFP tumor section. Scale bars represent 50μm.

Supplementary Figure 3. Gene set enrichment analysis (GSEA) plots of published gene signatures for molecular subtypes of human glioblastoma and medulloblastoma for genes

differentially regulated in p53EPS compared to control injected brains[6,19,32]. Normalized Enrichment Scores (NES) and False Discovery Rates (FDR) are indicated.

Supplementary Figure 4. Quantitative real-time PCR analysis of neural stem cell (NSC) genes and genes associated with published inflammatory gene signatures identified using bulk RNA sequencing. Gene expression in pooled *her4.1:*mScarlet+/*gfap:*GFP+ FACS-sorted cells relative to non-tumor control brain tissue. *p<0.01, **p<0.001, n=3, Student's t-test.

Supplementary Figure 5. Quantitative real-time PCR analysis of *irf7* CRISPR/Cas9-injected **(A)** and *irf8* CRISPR/Cas9-injected p53EPS **(B)**. Gene expression is represented relative to control p53EPS tumor-burdened whole brains. At least 5 tumor-burdened brains were pooled for each cohort and expression was normalized to mScarlet mRNA expression to account for differences in tumor size. *p<0.01, Student's t-test.

Supplementary Figure 6. Neutral red (phagocyte) foci in control and *irf8* CRISPR/Cas9-injected zebrafish larvae at 8 dpf. *p<0.01, n=4 fish for each cohort, Student's t-test.

Supplementary Figure 7. (A) Quantitative real-time PCR analysis of neural stem cell (NSC) genes and inflammation genes in non-tumor control brains, pooled p53EPS-burdened brains and pooled brains engrafted with p53EPS tumor cells at 20 dpf. *p<0.01 compared to non-tumor control whole brain tissue, Student's t-test. **(B)** Quantitative real-time PCR analysis of neural stem cell (NSC) genes and inflammation genes at 20 dpf in primary transplanted (1T) p53EPS-burdened brains injected with vehicle control liposomes (1T p53EPS) and Clodrosomes at 2 dpf. At least 5 tumor-burdened brains were pooled for each cohort and expression was normalized

to mScarlet mRNA expression to account for differences in tumor size. *p<0.01 compared to 1T p53EPS, Student's t-test.

Supplementary Movie 1. Time-lapse confocal images of p53EPS brain at 12 dpf in transgenic Tg(*mpeg1.1*:GFP) background.

Supplementary Movie 2. Time-lapse confocal images of individual *her4.1:*mScarlet+ p53EPS and *mpeg1.1:*EGFP+ cells at 12 dpf.

Supplementary Figure 1

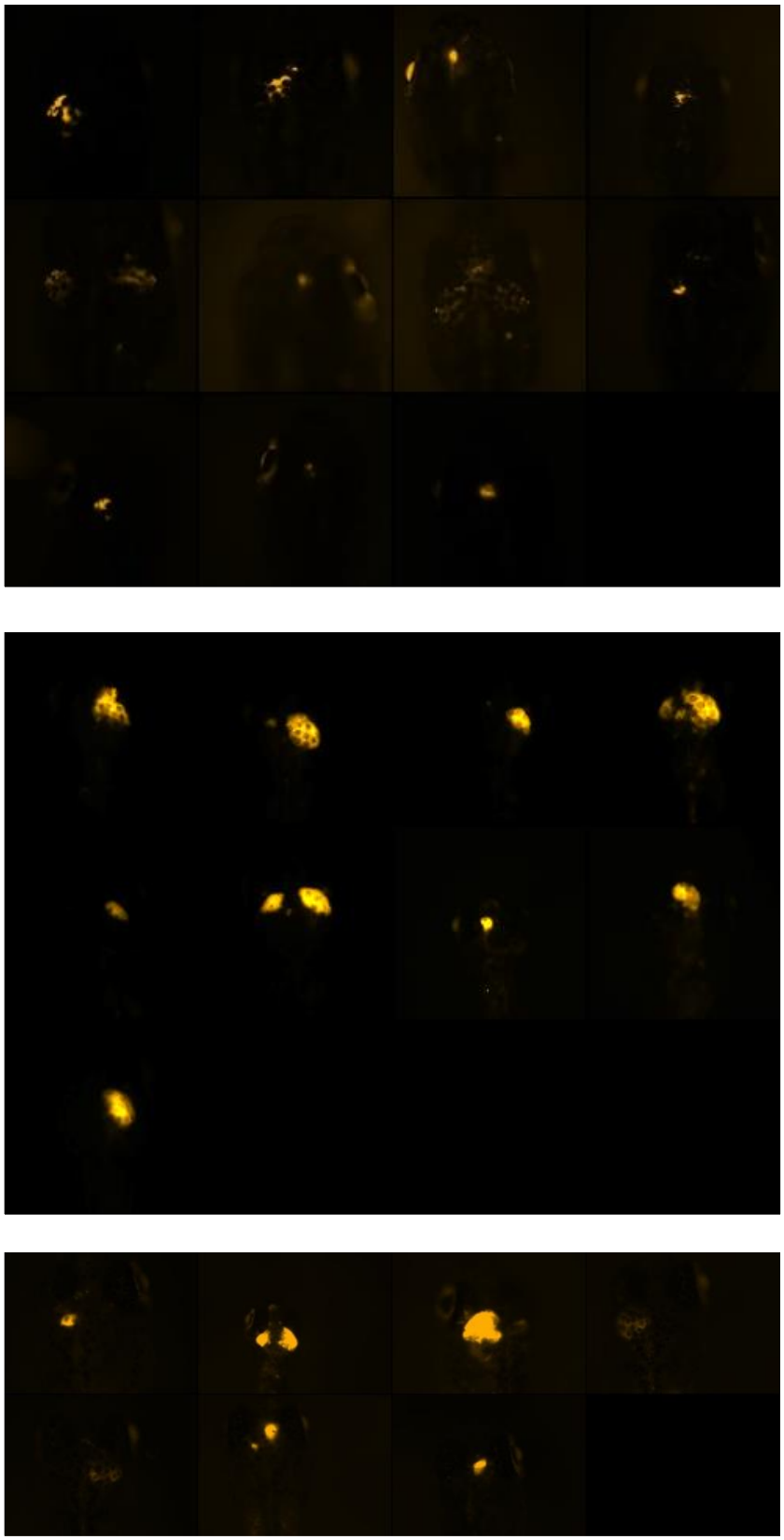

Supplementary Figure 2

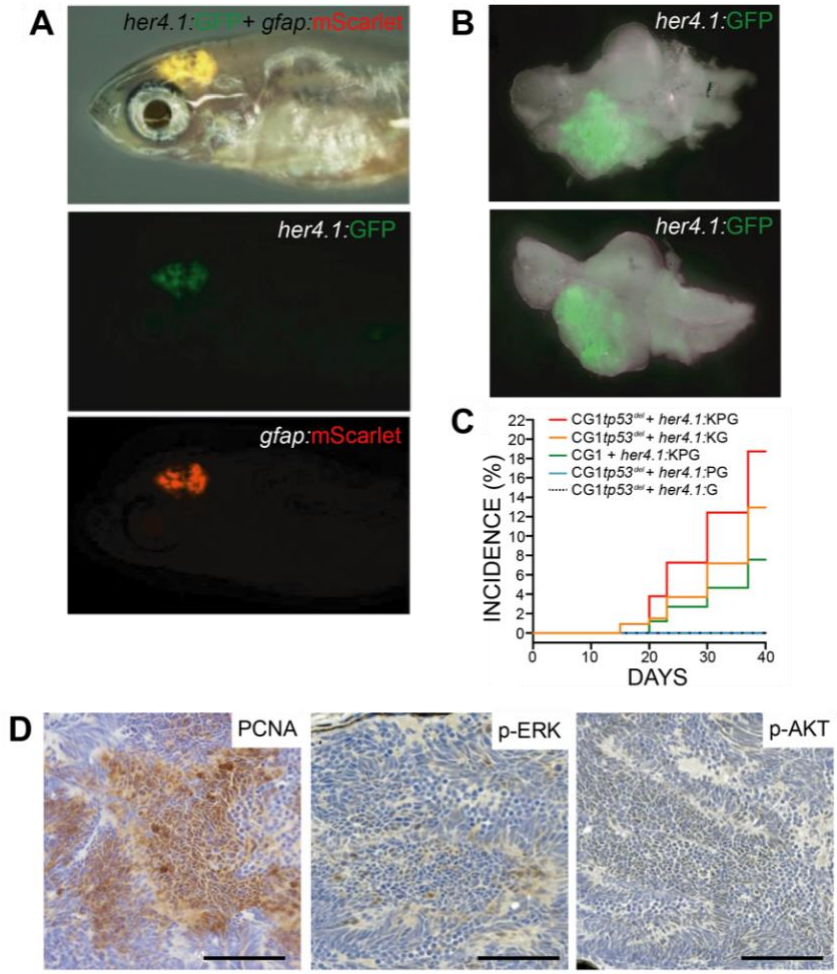

Supplementary Figure 3

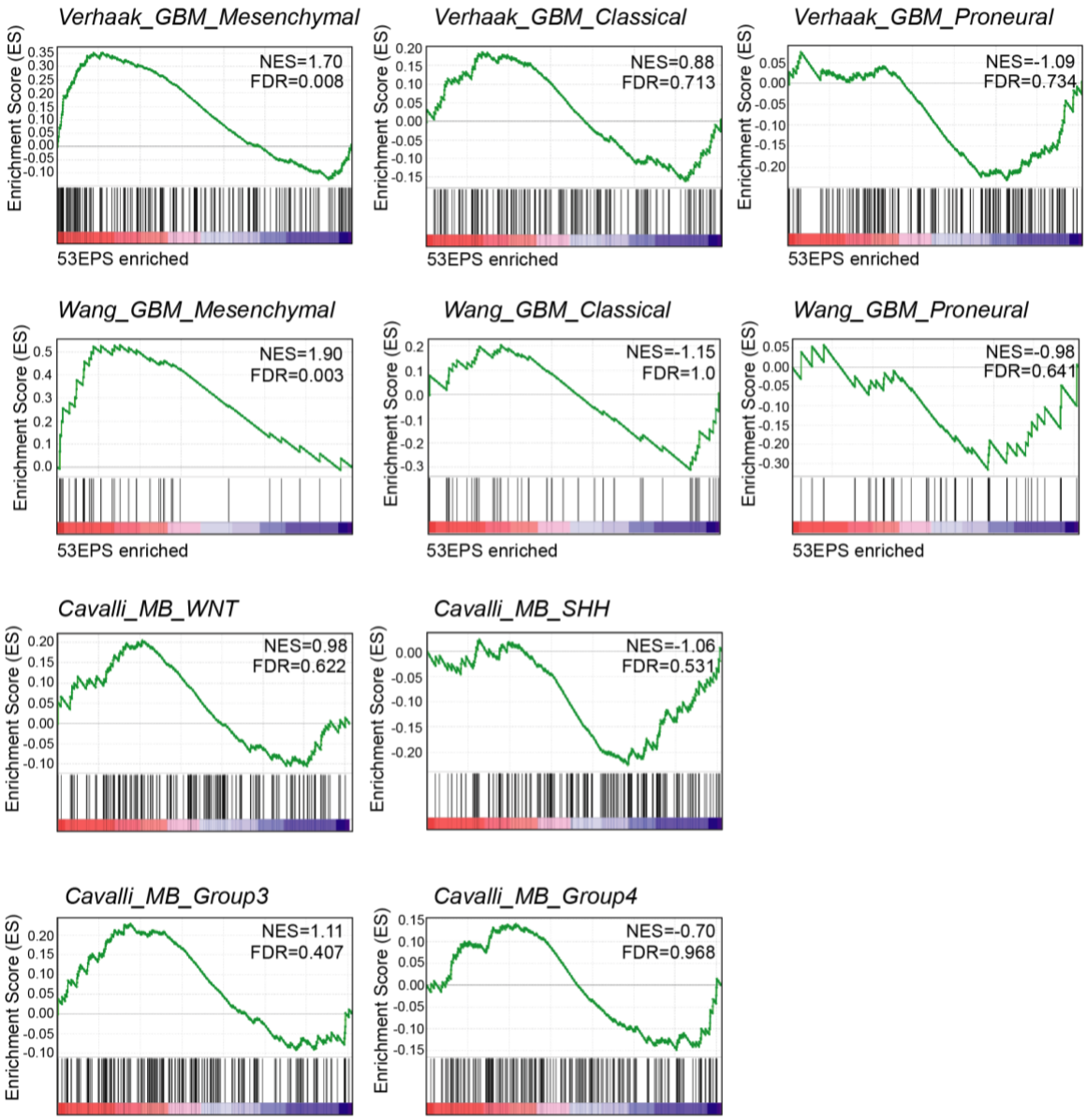

Supplementary Figure 4

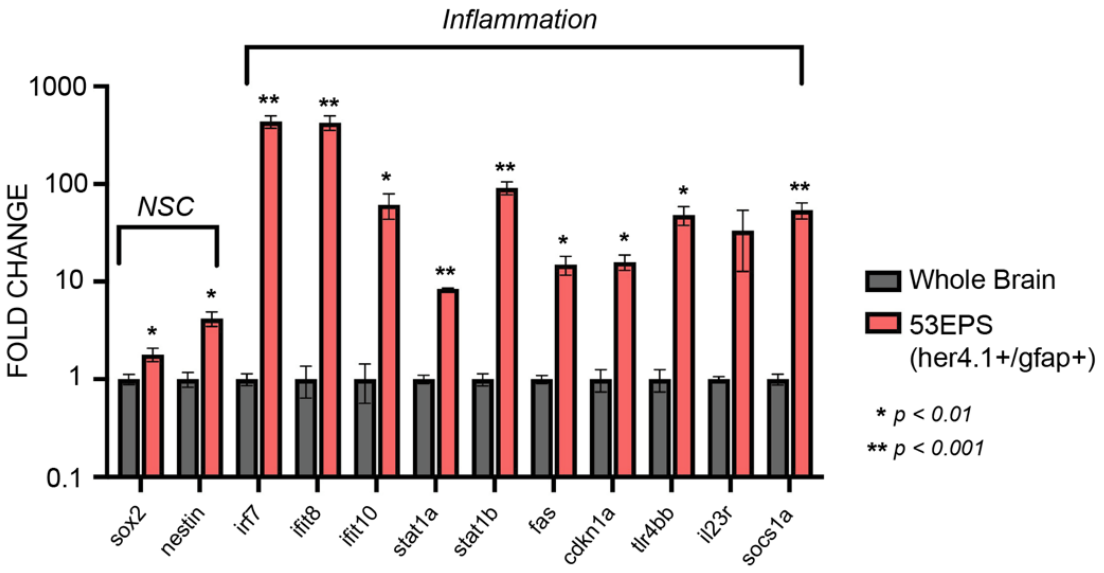

Supplementary Figure 5

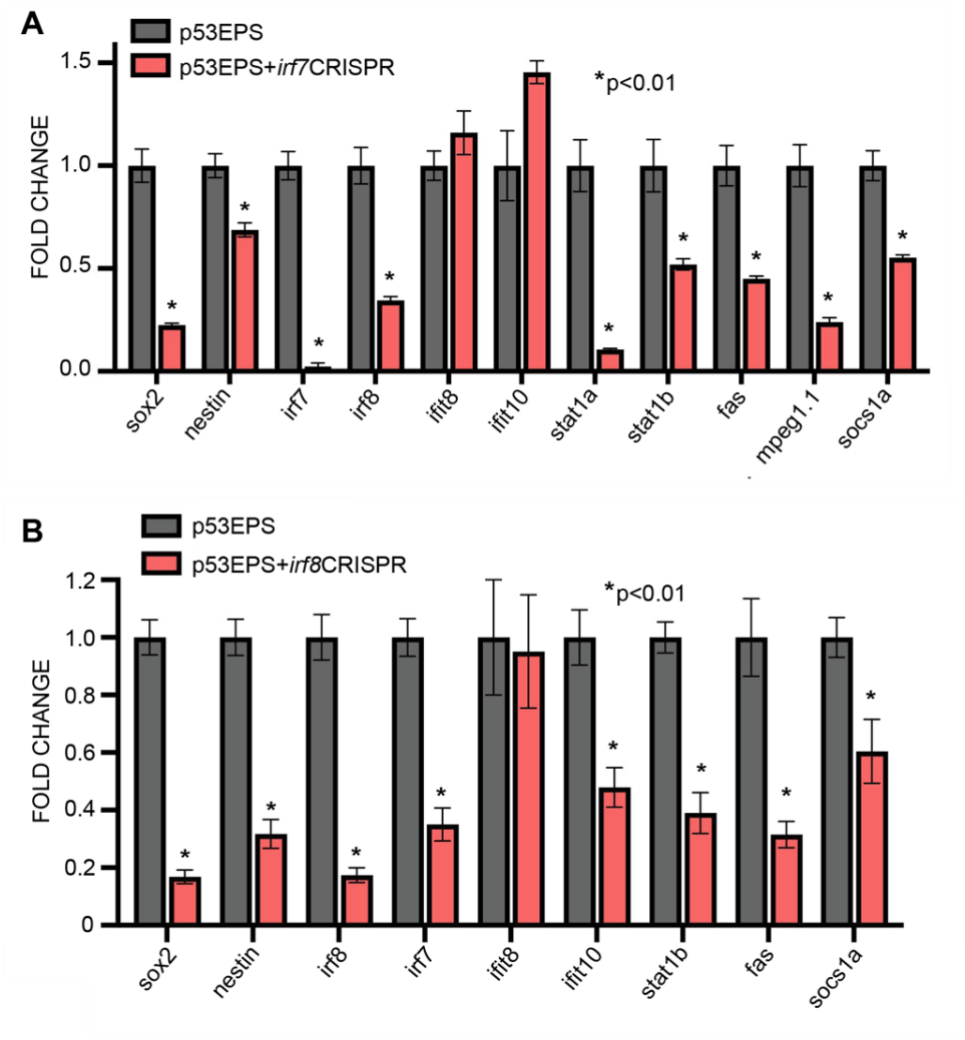

Supplementary Figure 6

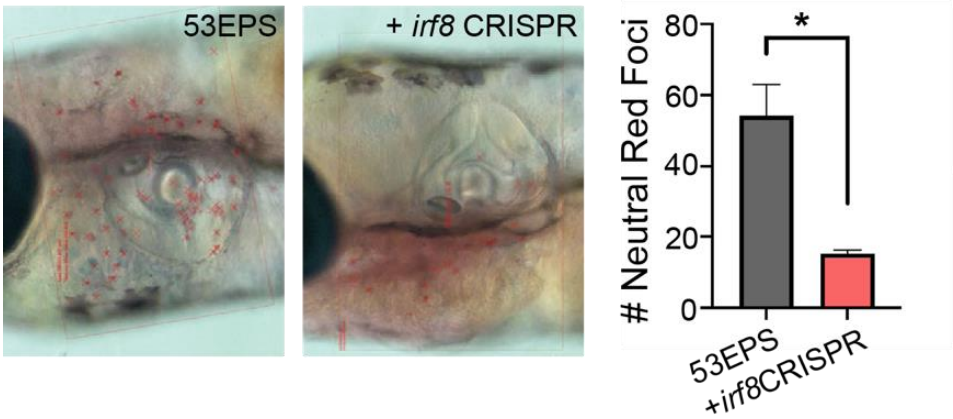
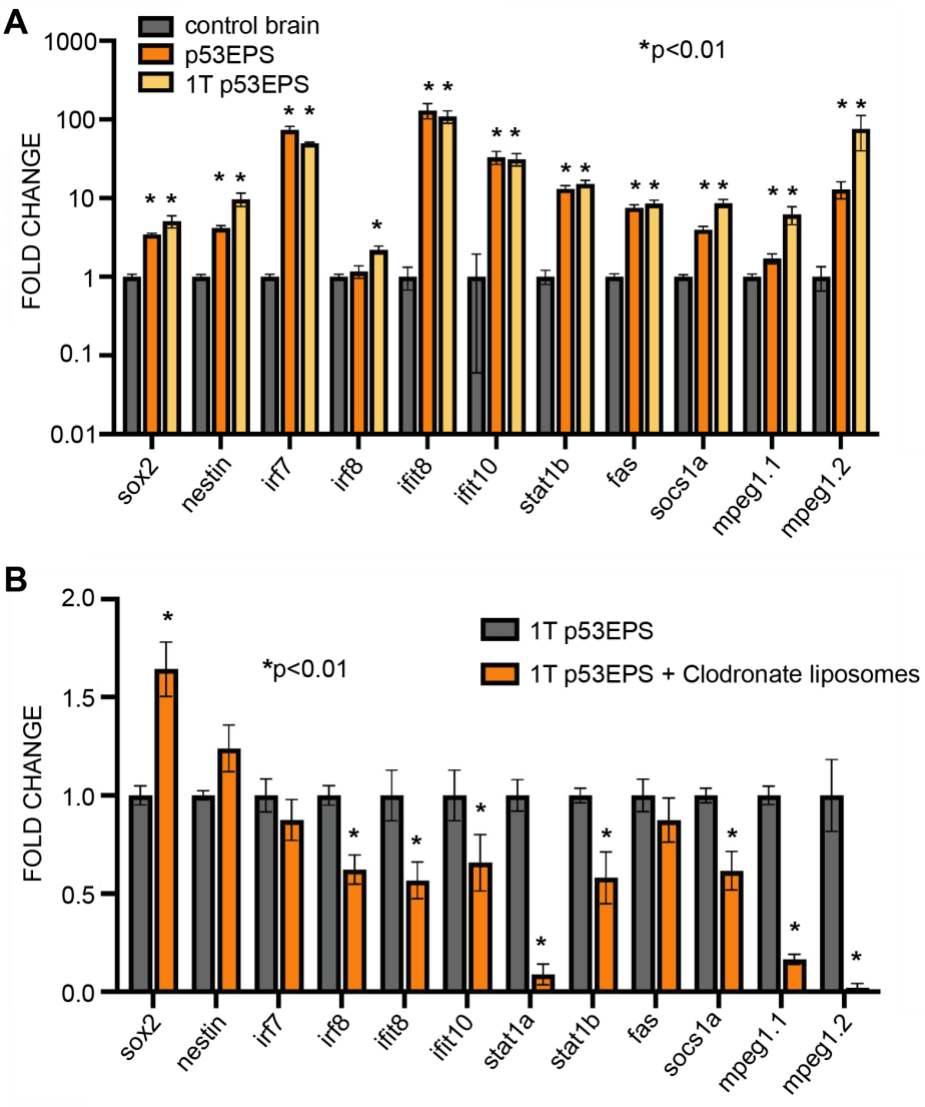
Supplementary Figure 7